In Search for Mononuclear Helical Lanthanide Building Blocks with Predetermined Properties: Triple-Stranded Helical Complexes with *N,N,N′,N′*-Tetraethylpyridine-2,6-dicarboxamide

Fabien Renaud, Claude Piguet,* Gérald Bernardinelli, Jean-Claude G. Bünzli,* and Gérard Hopfgartner

Abstract: The ligand *N,N,N′,N′*-tetraethylpyridine-2,6-dicarboxamide ($\mathbf{L^9}$) reacts with trivalent lanthanide ions (Ln^{III}) to give stable mononuclear triple-stranded helical complexes $[Ln(\mathbf{L^9})_3]^{3+}$ (Ln = La to Lu). The crystal and molecular structures of $[La(\mathbf{L^9})_3](ClO_4)_3 \cdot 2.5C_2H_5CN$ (**8**) and $[Eu(\mathbf{L^9})_3](TfO)_3 \cdot 2THF$ (**9**) show that the three ligand strands are each meridionally tricoordinated to produce a pseudo-tricapped trigonal prismatic arrangement of the nine donor atoms (six amide O and three pyridine N) around Ln^{III}. The distortions in the La^{III} coordination sphere of **8** are more significant than for Eu^{III} in **9**, and the photophysical studies on Eu-doped (2%) La, Gd, and Lu complexes confirm a better structural match of $\mathbf{L^9}$ for the heavy Ln^{III} ions. The separation of contact and pseudo-contact contributions to the induced lanthanide paramagnetic NMR shifts in $[Ln(\mathbf{L^9})_3]^{3+}$ shows that the triple-helical structure is maintained in acetonitrile, but a minor structural change relative to that observed in the solid state occurs between Tb^{III} and Er^{III} leading to two distinct isostructural series for Ln = La–Tb and Ln = Er–Lu. The origin of this effect together with its consequences for the dynamic helical ($P \rightleftharpoons M$) interconversion and stability of $[Ln(\mathbf{L^9})_3]^{3+}$ in solution are discussed. A detailed investigation of the emission properties of $[Ln(\mathbf{L^9})_3]^{3+}$ (Ln = Eu, Tb) shows that mixed pyridine–carboxamide ligands can be used to simultaneously optimize the structural and photophysical properties in mononuclear triple-helical lanthanide building blocks.

Keywords
carboxamides · helical structures · lanthanides · luminescence · tridentate ligands

Introduction

As a result of their particular $4f^n$ electronic configurations, the trivalent lanthanide ions Ln^{III} exhibit atom-like magnetic and spectroscopic properties in complexes which make them suitable for the development of fascinating molecular and supramolecular devices.[1, 2] Recently particularly rapid development has been observed in 1) the design of luminescent probes for time-resolved fluoroimunoassays[3] and DNA-labeling,[4] 2) the design of magnetic probes as contrast agents in magnetic resonance imaging[5] and NMR shift reagents,[6] and 3) the specific cleavage of DNA and RNA with lanthanide macrocycles.[7] These applications make use of specific properties of the lanthanide complexes achieved through a precise structural and electronic control of the lanthanide coordination sites. However, the selective recognition and incorporation of Ln^{III} into organized architectures as a means of simultaneously controlling the structural (symmetry, stability, accessibility) and electronic (donor atoms, spin delocalization, energy levels) properties of the metal remains a challenge in supramolecular chemistry because Ln^{III} ions display 1) large and variable coordination numbers, 2) little stereochemical preference, and 3) very similar coordination behavior along the complete series, slightly modified by a contraction in the ionic radii between La^{III} and Lu^{III} of around 15%.[8] Attempts to use the lock-and-key principle[9] with preorganized macrocycles, branched macrocycles,[2, 10] and macrobicyclic cryptands possessing bidentate binding units[10–12] have led to lanthanide complexes where Ln^{III} is only partially recognized and protected by these rigid receptors. In order to allow a better match between the binding units of the receptor and Ln^{III}, covalent podands made of flexible tripods connected to semi-rigid side arms have been developed.[13–15] In one case, a flexible podand has been shown to exhibit an unprecedented selectivity for the heavier lanthanides in water.[14] An alternative approach, based on

[*] C. Piguet, F. Renaud
Department of Inorganic, Analytical and Applied Chemistry
University of Geneva, 30 quai E. Ansermet, 1211 Geneva 4 (Switzerland)
Fax: Int. code +(4122)702-6069
e-mail: claude.piguet@chiam.unige.ch
G. Bernardinelli
Laboratory of X-ray Crystallography
24 quai E. Ansermet, 1211 Geneva 4 (Switzerland)
J.-C. G. Bünzli
Institute of Inorganic and Analytical Chemistry
University of Lausanne, BCH 1402, 1015 Lausanne (Switzerland)
G. Hopfgartner
F. Hoffmann-La Roche, Pharmaceuticals Division
Department of Drug Metabolism and Kinetics, 4070 Basle (Switzerland)

0947-6539/97/0310-1646 $ 17.50+.50/0

the concept of induced fit,[16] uses the rigid tridentate aromatic ligands $\mathbf{L}^i$ ($i = 0$–4) as selective receptors for Ln^{III}.[17–19] In triple-stranded helical lanthanide complexes $[Ln(\mathbf{L}^i)_3]^{3+}$, the three ligands display sizable π–π stacking interactions, which control the size of the coordination sphere around Ln^{III}. Through the judicious choice of substituents on the strands, the electronic,[18] thermodynamic,[17, 19] and structural[17] properties of the $[Ln(\mathbf{L}^i)_3]^{3+}$ building blocks can be fine-tuned. These tridentate binding units have been successfully introduced into homotopic ($\mathbf{L}^5$) and heterotopic ($\mathbf{L}^6$) segmental ligands,[20, 21] which have in turn been used to prepare homodinuclear f–f triple-stranded helicates $[Ln_2(\mathbf{L}^5)_3]^{6+}$[21] and heterodinuclear d–f noncovalent lanthanide podates (HHH)-$[LnM(\mathbf{L}^6)_3]^{5+}$ (M = Fe,[22] Zn[23]). The replacement of the terminal benzimidazole unit in $\mathbf{L}^6$ by a carboxamide unit in $\mathbf{L}^7$, which is known to favor lanthanide complexation and ligand → Eu^{III} energy transfers,[12, 24] provides the heterodinuclear triple-helical noncovalent podate (HHH)-$[EuZn(\mathbf{L}^7)_3]^{5+}$ where the nonacoordinated Eu^{III} is water-resistant and 10^3–10^4 more luminescent than in (HHH)-$[EuZn(\mathbf{L}^6)_3]^{5+}$.[25]

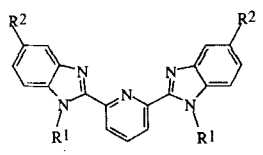

L^i	R^1	R^2
L^0	H	H
L^1	Me	H
L^2	Et	H
L^3	Et	Me
L^4	3,5-$(MeO)_2C_6H_3CH_2$	H

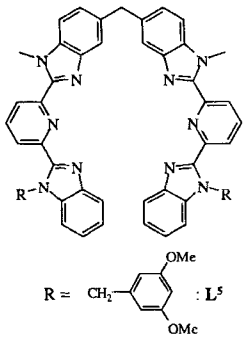

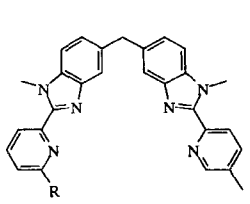

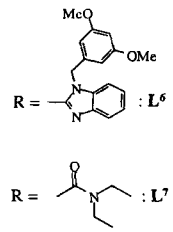

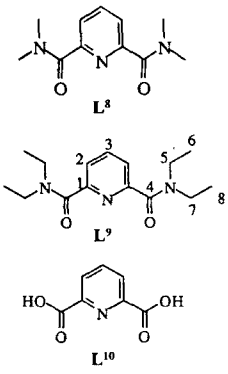

Dipicolinic acid $\mathbf{L}^{10}$ is a good candidate for the design of triple-stranded Ln^{III} building blocks since it forms stable and strongly luminescent complexes $[Ln(\mathbf{L}^{10} - 2H)_3]^{3-}$ in water.[26–28] However, only limited structural and electronic control of the lanthanide coordination sphere is achievable in dipicolinate derivatives, because no substituents can be connected to the carboxylic side arms. Carboxamide derivatives such as $\mathbf{L}^{8-9}$ are promising ligands for the investigation of subtle electronic and steric effects induced by the wrapped strands in triple-helical lanthanide building blocks. Although carboxamide side arms have been extensively used in Ln^{III} complexes with branched macrocycles[29] and multidentate chelates,[30] complexes of $\mathbf{L}^{8-9}$ have been studied in detail only with d-block metal ions,[31] and no complete investigation has been reported for Ln^{III}. To the best of our knowledge, 1:3 complexes $[Ln(\mathbf{L}^i)_3](ClO_4)_3$ ($i = 8$, 9) have been isolated in the solid state and briefly characterized by elemental analysis and IR spectroscopy, which suggested that the Ln^{III} ions are nonacoordinated as found in $[Ln(\mathbf{L}^{10} - 2H)_3]^{3-}$.[32]

In this paper, we present the detailed coordination behavior of $\mathbf{L}^9$ (which possesses diastereotopic methylene protons to facilitate ^1H NMR analysis)[33] with the Ln^{III} series. Particular attention has been focused on the structural, thermodynamic, photophysical, and electronic properties of the 1:3 complexes $[Ln(\mathbf{L}^9)_3]^{3+}$ in the solid state and in solution to investigate the possible fine-tuning of the lanthanide coordination site induced by the carboxamide side arms.

Results and Discussions

Synthesis of the complexes: Reaction of 3 equiv of $\mathbf{L}^9$ with 1 equiv of $Ln(TfO)_3 \cdot nH_2O$ ($n = 0.3$–2.2; Ln = Y, Sm, Eu, Gd, Tb, Lu; TfO = trifluoromethanesulfonate) in THF followed by crystallization produced microcrystalline powders in almost quantitative yields, with elemental analyses corresponding to $[Ln(\mathbf{L}^9)_3](TfO)_3 \cdot H_2O$ (Ln = Y, **2**; Sm, **4**; Eu, **5**; Gd, **6**; Tb, **7**; Lu, **3**). Pure 1:3 complexes could not be obtained for the larger lanthanides (Ln = La–Nd) under similar experimental conditions. The elemental analyses suggest the formation of mixtures of 1:2 and 1:3 complexes. Microcrystalline $[La(\mathbf{L}^9)_3](ClO_4)_3$ (**1**) could be isolated quantitatively from a propionitrile solution containing 1 equiv of $La(ClO_4)_3 \cdot 5.4H_2O$ and 4 equiv of $\mathbf{L}^9$. The IR spectra in KBr of complexes **1**–**7** display the typical bands associated with the coordinated ligands[32] together with uncoordinated TfO^-[34] and ClO_4^-.[35]

Crystal and molecular structures of $[La(\mathbf{L}^9)_3](ClO_4)_3 \cdot 2.5C_2H_5CN$ (8) and $[Eu(\mathbf{L}^9)_3](TfO)_3 \cdot 2THF$ (9): X-ray quality crystals of **8** and **9** were obtained by the same procedure as described above, but the prisms were not separated from the mother liquor. Both structures consist of a discrete $[Ln(\mathbf{L}^9)_3]^{3+}$ cations and disordered uncoordinated anions and solvent molecules. In each cation, the three tridentate ligands $\mathbf{L}^9$ are meridionally tricoordinated to and helically wrapped around the metal ion producing pseudo-D_3 triple-helical complexes analogous to those reported for $[Ln(\mathbf{L}^{10} - 2H)_3]^{3-}$.[26] Selected bond lengths and angles are given in Table 1. Figure 1 shows ORTEP[36] views of the cations along their pseudo-C_3 axis with the atomic numbering schemes around Ln^{III}, and Figure 2 shows stereoviews of both cations in similar orientations.

The Ln^{III} ions in $[Ln(\mathbf{L}^9)_3]^{3+}$ are nonacoordinated producing distorted pseudo-tricapped trigonal prismatic coordination polyhedrons where the six O atoms of the carboxamide groups occupy the vertices of the trigonal prism and the N atoms of the pyridine rings occupy the capping positions, forming an equatorial plane containing the lanthanide ion. In $[Eu(\mathbf{L}^9)_3]^{3+}$, the cation is located about a crystallographic twofold axis passing through Eu, N1b, and C3b. This twofold axis is perpendicular to the pseudo-C_3 axis, and there is thus only limited deviation from an idealized D_3 symmetry (except for the ethyl groups). The two facial planes defined by the two distal tripods O1a/

  0947-6539/97/0310-1647 $ 17.50+.50/0

Table 1. Structural data for complexes $[La(\mathbf{L^9})_3](ClO_4)_3 \cdot 2.5\,C_2H_5CN$ (**8**) and $[Eu(\mathbf{L^9})_3](TfO)_3 \cdot 2\,THF$ (**9**).

a) Selected bond lengths (Å) and bite angles (°).

	Complex **8**			Complex **9**	
	Ligand a	Ligand b	Ligand c	Ligand a	Ligand b [a]
Ln–O1	2.470(5)	2.496(6)	2.527(6)	2.426(5)	2.392(5)
Ln–N1	2.679(7)	2.731(7)	2.696(7)	2.547(6)	2.569(9)
Ln–O2	2.525(5)	2.501(5)	2.501(6)	2.405(5)	
O1-Ln-N1	60.9(2)	61.4(2)	62.2(2)	63.3(2)	62.6(1)
N1-Ln-O2	61.7(2)	60.9(2)	60.4(2)	63.3(2)	
O1-Ln-O2	122.4(2)	122.3(2)	122.3(2)	126.4(2)	125.2(2)

b) Angles N-Ln-N, O-Ln-N, and O-Ln-O.

Complex **8**		Complex **9**	
N1a-La-N1b	130.2(2)	N1a-Eu-N1b	119.1(1)
N1a-La-N1c	111.8(2)	N1a-Eu-N1a′	121.8(2)
N1b-La-N1c	118.0(2)		
O1a-La-N1b	134.4(2)	O1a-Eu-N1b	139.0(1)
O2a-La-N1c	135.0(2)	O1a-Eu-N1a′	73.4(2)
O2b-La-N1a	141.2(2)	O2a-Eu-N1b	74.5(1)
O1c-La-N1a	136.3(2)	O2a-Eu-N1a′	135.3(1)
O1c-La-N1b	72.3(2)	O1b-Eu-N1a	74.6(2)
O1a-La-N1c	73.4(2)	O1b′-Eu-N1a	135.6(2)
O2a-La-N1b	82.5(2)		
O1b-La-N1a	81.6(2)		
O2c-La-N1a	73.2(2)		
O1b-La-N1c	138.8(2)		
O2b-La-N1c	71.9(2)		
O2c-La-N1b	132.9(2)		
O1a-La-O1b	81.3(2)	O2a-Eu-O1b′	76.6(2)
O1a-La-O2c	92.1(2)	O1a-Eu-O1b	81.3(2)
O2a-La-O2b	87.9(2)	O1a-Eu-O1a′	82.0(2)
O2a-La-O1c	154.8(2)	O1a-Eu-O1b′	147.8(2)
O1b-La-O2c	153.8(2)	O2a-Eu-O1b	89.1(2)
O2b-La-O2c	76.7(2)	O2a-Eu-O1a′	79.1(2)
O1a-La-O2b	144.6(2)	O1a-Eu-O2a′	148.9(2)
O1a-La-O1c	77.0(2)		
O2a-La-O1b	86.1(2)		
O2a-La-O2c	76.2(2)		
O1b-La-O1c	81.0(2)		
O2b-La-O1c	81.0(2)		

[a] The complex **9** is located about a twofold axis with Eu, N1b, and C3b in special position 4e; the other part of the complex is obtained by the symmetry operation $1-x, y, {}^1/_2-z$.

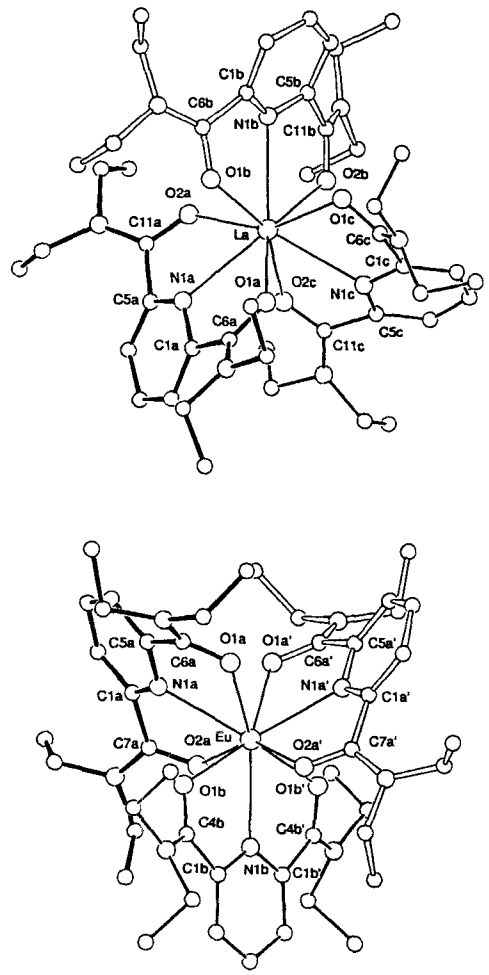

Figure 1. Atomic numbering scheme for a) $[La(\mathbf{L^9})_3]^{3+}$ (**8**) and b) $[Eu(\mathbf{L^9})_3]^{3+}$ (**9**) along the pseudo-C_3 axis.

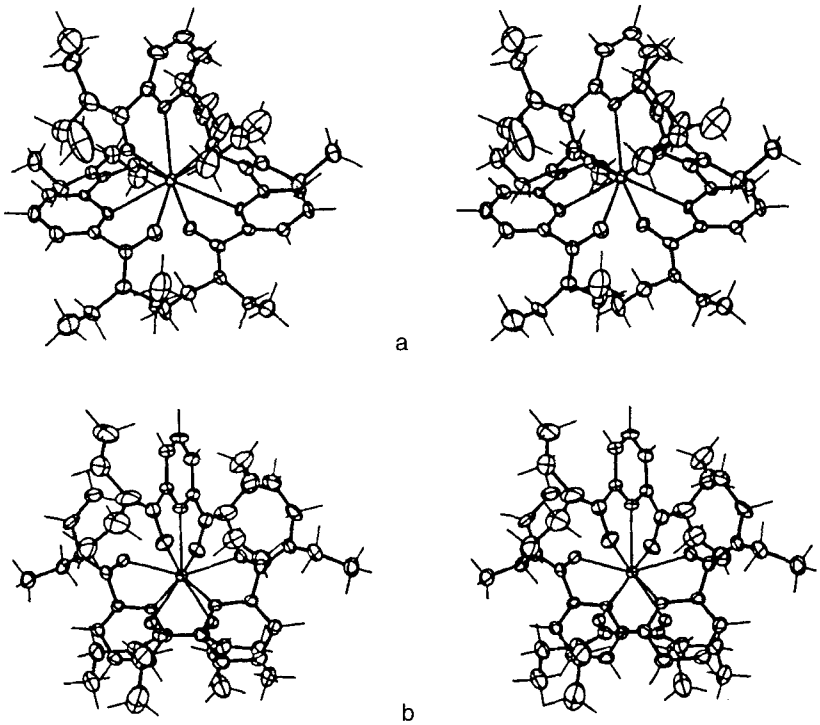

Figure 2. ORTEP[36] stereoviews of a) $[La(\mathbf{L^9})_3]^{3+}$ (**8**) and b) $[Eu(\mathbf{L^9})_3]^{3+}$ (**9**) (ellipsoids at 50% probability level).

O1b/O2a′ and O1a′/O1b′/O2a are almost parallel (interplane angle = 3.5°) and separated by 3.26 Å, a distance significantly shorter than found for $[Eu(\mathbf{L^{10}}-2H)_3]^{3-}$ (3.44 Å); this indicates a significant flattening of the trigonal prism along the pseudo-C_3 axis.[26] A detailed geometrical analysis of the coordination sphere based on the ϕ, θ_i, and ω_i angles depicted in Scheme 1[18, 25] is reported in Table 2. These measure 1) the average bending of the two distal tripods connected to Eu (ϕ), 2) the flattening of the pseudo-trigonal prism along the pseudo-C_3 axis (θ_i), and 3) the deformation of the trigonal prism defined by the distal tripods toward the octahedron (ω_i). The ϕ angles for $[Eu(\mathbf{L^{10}}-2H)_3]^{3-}$ and $[Eu(\mathbf{L^9})_3]^{3+}$ (178–180°) do not deviate significantly from the expected value for a perfect trigonal prism ($\phi = 180°$) and indicate only a small bending of the two distal tripods. The θ_i angles in $[Eu(\mathbf{L^9})_3]^{3+}$ (46–49°) are slightly

0947-6539/97/0310-1648 $ 17.50+.50/0 *Chem. Eur. J.* **1997**, *3*, No. 10

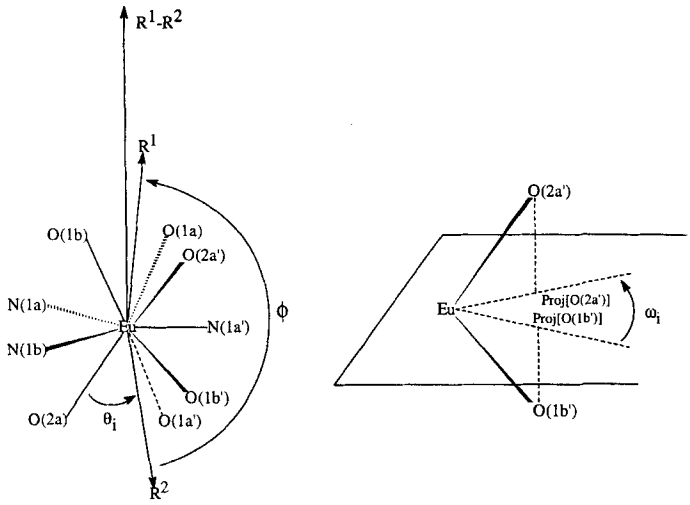

Scheme 1. Definition of the ϕ, θ_i, and ω_i angles in the coordination sphere of the lanthanide complexes.

Table 2. Selected angles (°) [a] for the Ln^{III} coordination spheres in $[La(\mathbf{L^9})_3](ClO_4)_3 \cdot 2.5C_2H_5CN$ (**8**), $[Eu(\mathbf{L^9})_3](TfO)_3 \cdot 2THF$ (**9**), and $Cs_3[Eu(\mathbf{L^{10}} - 2H)_3] \cdot 9H_2O$. Top: ϕ; middle: θ_i (distal tripods); bottom: interligand ω_i angles [b].

	8		**9**	$Cs_3[Eu(\mathbf{L^{10}} - 2H)_3]$ [c]
R^1-La-R^2	176	R^1-Eu-R^2	178	178
R^1-La-O1a	47	R^1-Eu-O1a	49	45
R^1-La-O1b	50	R^1-Eu-O1b	47	45
R^1-La-N1c	46	R^2-Eu-O2a	46	46
R^2-La-O2a	50			
R^2-La-O2b	51			
R^2-La-O2c	43			
proj(O1a)-La-proj(O2c)	20	proj(O1a)-Eu-proj(O1a')	15	19
proj(O1c)-La-proj(O2b)	18	proj(O1b)-Eu-proj(O2a)	17	18
proj(O2a)-La-proj(O1b)	25	proj(O1b')-Eu-proj(O2a')	17	18
proj(N1a)-La-proj(N1b)	130	proj(N1a)-Eu-proj(N1b)	119	121
proj(N1a)-La-proj(N1c)	112	proj(N1a)-Eu-proj(N1a')	122	120
proj(N1b)-La-proj(N1c)	118	proj(N1a')-Eu-proj(O1b')	119	120

[a] For the definition of ϕ, θ_i, and ω_i see Scheme 1 and ref. [18]; the error in the angles is typically $\leq 1°$. [b] proj(O*i*) is the projection of O*i* along the R^1-R^2 direction onto a perpendicular plane passing through the lanthanide atom; the resulting vectors R^1 and R^2 correspond to: R^1 = La–O1a + La–O1b + La–O1c or R^1 = Eu–O1a + Eu–O1b + Eu–O2a′ and R^2 = La–O2a + La–O2b + La–O2c or R^2 = Eu–O1a′ + Eu–O1b′ + Eu–O2a. [c] In the crystal structure of $Cs_3[Eu(\mathbf{L^{10}} - 2H)_3] \cdot 9H_2O$, the anion $[Eu(\mathbf{L^{10}} - 2H)_3]^{3-}$ is located about a crystallographic twofold axis as similarly observed for $[Eu(\mathbf{L^9})_3]^{3+}$ [26].

larger than those found in $[Eu(\mathbf{L^{10}} - 2H)_3]^{3-}$ (45–46°), in agreement with the observed larger separation between the facial planes in the latter complex. The ω_i angles between the eclipsed oxygen donor atoms of the distal tripods (14–17°) exemplify the typical distortion from the ideal trigonal prism ($\omega_i = 0°$) toward the octahedron ($\omega_i = 60°$) induced by constrained tridentate ligands in mononuclear lanthanide helicates, as previously observed for $[Eu(\mathbf{L^1})_3]^{3+}$ (10°)[17] and $[Eu(\mathbf{L^3})_3]^{3+}$ (13–14°).[18] The tridentate ligand strand b lies about the twofold axis in $[Eu(\mathbf{L^9})_3]^{3+}$ and consequently adopts a twist conformation of the carbonyl side arms with Eu^{III} in the plane of the coordinated pyridine ring. The two other coordinated tridentate ligand strands (a and a′) display bent conformations with Eu^{III} located significantly out of the plane of the coordinated pyridine rings (1.00 Å, Figure 2). Nevertheless, the Eu–N bond lengths (2.55–2.57 Å) are close to the values reported for Eu–N(pyridine)[17, 18, 21, 25] and similar to those found in $[Eu(\mathbf{L^{10}} - 2H)_3]^{3-}$ (2.52–2.54 Å).[26] The Eu–O(amide) bonds in $[Eu(\mathbf{L^9})_3]^{3+}$ (2.39–2.43 Å) are slightly shorter than the Eu–O(carboxylate) bonds in $[Eu(\mathbf{L^{10}} - 2H)_3]^{3-}$ (2.43–2.45 Å),[26] but fall within the expected range.[25, 37] Calculation of the Eu^{III} ionic radius by using Shannon's definition[38] with $r(N) = 1.46$ Å and $r(O) = 1.31$ Å gives 1.09 Å, a smaller value than expected for nonacoordinated Eu^{III} (1.12 Å)[8] and than found for $[Eu(\mathbf{L^1})_3]^{3+}$ and $[Eu(\mathbf{L^3})_3]^{3+}$ (1.13 Å)[17, 18] and for $[Eu(\mathbf{L^{10}} - 2H)_3]^{3-}$ (1.12 Å). This result suggests that there is a slight contraction of the Eu^{III} coordination sphere induced by the wrapped tridentate ligands $\mathbf{L^9}$.

The coordination sphere around La^{III} in $[La(\mathbf{L^9})_3]^{3+}$ is more distorted and displays significant deviations from the ideal D_3 symmetry. The two distal oxygen tripods defining the triangular faces of the trigonal prism are more tilted (6.3°) than in $[Eu(\mathbf{L^9})_3]^{3+}$, but the three N atoms of the pyridine rings capping the lateral faces of the prism still form an intermediate plane containing the metal atom. However, these pyridine rings are no longer equally distributed around La^{III}, and the N1a-La-N1b angle (130.2(2)°) is significantly larger than 120°. The flattening of the two tripods along the pseudo-C_3 axis (θ_i) is similar for both cations $[Ln(\mathbf{L^9})_3]^{3+}$ (Ln = La, Eu; Table 2), but the ω_i angles between the eclipsed oxygen atoms in $[La(\mathbf{L^9})_3]^{3+}$ (18–25°) reveal an increased deformation of the trigonal prism toward the octahedron for the larger La^{III}. A similar trend has been reported for $[Ln(\mathbf{L^{10}} - 2H)_3]^{3-}$ on going from Lu to La.[26] However, the most striking distortion is associated with the severe tilting of the pyridine rings leading to 1) bent conformations of the meridionally tricoordinated ligands and 2) significant mismatches between the orientation of the nitrogen lone pairs of the pyridine rings and the La^{III} ion. Consequently, La^{III} lies significantly out of the plane of each pyridine ring (1.17–1.50 Å), and the La–N bond lengths (2.68–2.73 Å, average 2.70(2) Å) are 0.15 Å longer than those found in $[Eu(\mathbf{L^9})_3]^{3+}$; we expect an expansion of 0.09–0.10 Å on going from Eu^{III} to La^{III},[8] as observed for the Ln–O(amide) bonds (Table 1). These observations indicate that steric constraints in the ligand backbone force the N atoms of the pyridine rings to move away to accommodate the large La^{III} ion in the cavity, leading to an uncompressed La^{III} ionic radius of 1.21 Å in $[La(\mathbf{L^9})_3]^{3+}$[38] (expected value for nonacoordinate La^{III}: 1.22 Å).[8] In contrast to triple-stranded helicates with polyaromatic ligands, which tend to give hexagonal close-packing of the crystals,[39] the $[Ln(\mathbf{L^9})_3]^{3+}$ cations in **8** and **9** do not show any remarkable arrangement or packing interactions.

Photophysical properties of $[La(\mathbf{L^9})_3](ClO_4)_3$ (1), $[Ln(\mathbf{L^9})_3](TfO)_3 \cdot H_2O$ (Ln = Eu, 5; Gd, 6; Tb, 7; Lu, 3) and $[Eu(\mathbf{L^9})_3](TfO)_3 \cdot 2THF$ (9): In acetonitrile, $\mathbf{L^9}$ shows a broad and asymmetric absorption band envelope centered around 37040 cm^{-1} (Table 3) and assigned to a combination $\pi \rightarrow \pi^*$ and $n \rightarrow \pi^*$ transitions,[18] by analogy with those found at lower

  0947-6539/97/0310-1649 $ 17.50+.50/0

Table 3. Ligand-centered absorptions in acetonitrile solution (293 K) and ligand-centered singlet- and triplet-state energies as determined from emission spectra of the solids at 77 K for $\mathbf{L^9}$ and its complexes $[Ln(\mathbf{L^9})_3]^{3+}$ (**1**–**7**).

Compd	Absorption $\pi \rightarrow \pi^* + n \rightarrow \pi^*$	Emission $^1\pi\pi^*$	Emission $^3\pi\pi^*$
$\mathbf{L^9}$	37040 (7160) [a]	[b]	[b]
$\mathbf{L^1}$ [c]	31150 (32000)	26040	21300
$[La(\mathbf{L^9})_3]^{3+}$ (**1**)	46950 (37130)	23500	20600
	41840 (33500)		
	35970 (31170)		
$[La(\mathbf{L^1})_3]^{3+}$ [c]	33450 (61590)	22220	18520
	28170 (47920)		
$[Gd(\mathbf{L^9})_3]^{3+}$ (**6**)	47170 (44900)	23500	20600
	42550 (36830)		
	35840 (35300)		
$[Gd(\mathbf{L^1})_3]^{3+}$ [c]	33445 (59950)	22220	18500
	27780 (48500)		
$[Y(\mathbf{L^9})_3]^{3+}$ (**2**)	47170 (45960)	[d]	[d]
	42370 (35660)		
	35840 (33400)		
$[Lu(\mathbf{L^9})_3]^{3+}$ (**3**)	47620 (45910)	[d]	[d]
	42550 (34490)		
	35840 (33010)		
$[Eu(\mathbf{L^9})_3]^{3+}$ (**5**)	47170 (39060)	[e]	[e]
	42370 (32000)		
	35840 (30510)		
$[Tb(\mathbf{L^9})_3]^{3+}$ (**7**)	47170 (42760)	[e]	[e]
	42370 (34760)		
	35830 (33590)		

[a] Energies are given for the maximum of the band envelope in cm^{-1} and the molar absorption coefficient (ε) is given in parentheses in $M^{-1}cm^{-1}$. [b] Too weak to be detected. [c] See ref. [17]. [d] Not measured. [e] Not detected due to $\mathbf{L^9} \rightarrow Ln^{III}$ energy transfer.

energy for $\mathbf{L^1}$ (31150 cm^{-1})[17] and $\mathbf{L^7}$ (33320 cm^{-1}).[25] Upon irradiation of $\mathbf{L^9}$ in the UV region (solid state, 77 K), we do not detect any significant emission. This points to the existence of efficient nonradiative deactivation pathways in the free ligand. The absorption spectra are strongly modified upon complexation, and irradiation of $[La(\mathbf{L^9})_3](ClO_4)_3$ (**1**) and $[Gd(\mathbf{L^9})_3](TfO)_3 \cdot H_2O$ (**6**) at 28400 cm^{-1} (solid state, 77 K) results in a faint luminescence from the $^1\pi\pi^*$ state characterized by a broad band centered at 23500 cm^{-1}, as previously reported for $[Ln(\mathbf{L^1})_3](ClO_4)_3$ (Ln = La, Gd).[17, 18] This assignment is corroborated by the almost complete disappearance of the broad emission band in the time-resolved emission spectra (delay time: 0.01–0.75 ms), which reveal a weak and structured band centered at 20600 cm^{-1} assigned to the phosphorescence of the $^3\pi\pi^*$ state. Compared to $[Ln(\mathbf{L^1})_3](ClO_4)_3$ (Ln = La, Gd), the ligand-centered $^1\pi\pi^*$ and $^3\pi\pi^*$ levels in **1** and **6** are blue-shifted by ca. 1500–2000 cm^{-1}.

The ligand-centered luminescence vanishes in the Eu (**5**) and Tb (**7**) complexes leading to typical Eu^{III}- and Tb^{III}-centered emissions.[11] This implies efficient intramolecular $\mathbf{L^9} \rightarrow Ln^{III}$ energy transfer processes in the 1:3 complexes (Figure 3). We

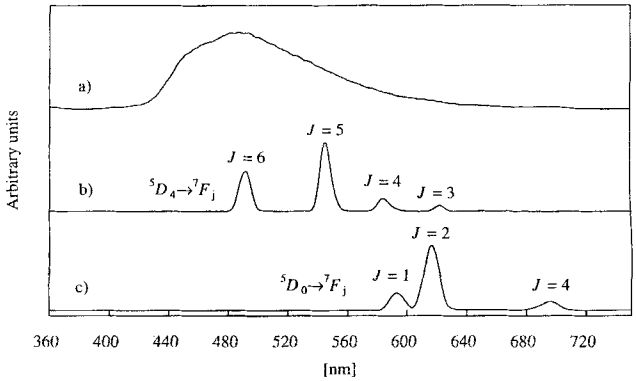

Figure 3. Low-resolution time-resolved (delay time = 0.01 ms) emission spectra of a) $[Gd(\mathbf{L^9})_3](TfO)_3 \cdot H_2O$ (**6**), b) $[Tb(\mathbf{L^9})_3](TfO)_3 \cdot H_2O$ (**7**), and c) $[Eu(\mathbf{L^9})_3](TfO)_3 \cdot H_2O$ (**5**) in the solid state at 77 K (λ_{exc} = 352 nm).

have used Eu^{III} as a luminescent structural probe to investigate the geometry of the coordination sites in **1**, **3**, **5**, **6**, and **9**. For the crystalline Eu complex **9**, the luminescence spectra obtained upon irradiation at 25190 cm^{-1} (via the excited states of the ligand) or through laser excitation in the $^5D_0 \leftarrow {}^7F_0$ transition are similar. There is no significant temperature dependence between 10 and 295 K, except for the expected intensity decrease at high temperature. Corrected and integrated intensities at 10 K for the $^5D_0 \rightarrow {}^7F_j$ ($j = 0, 1, 2, 3, 4$) transitions (Table 4) point to the lack of inversion center at the Eu^{III} site.[11] A close scrutiny of both emission and excitation spectra at 10 K in the region of the $^5D_0 \leftrightarrow {}^7F_0$ transition reveals the existence of a slightly unsymmetrical band with a major component at 17216 cm^{-1} (full width at half height (fwhh) = 2.4 cm^{-1}) and a weak shoulder at low energy probably associated with sites displaying a closely

Table 4. Corrected integrated intensities (I_{rel}) and main identified $Eu(^7F_j)$ energy levels (cm^{-1}, J=1–4, origin $^7F_0$) in $[Eu(\mathbf{L^9})_3](TfO)_3 \cdot 2THF$ (**9**), $[Eu(\mathbf{L^9})_3](TfO)_3 \cdot H_2O$ (**5**), and 2% Eu-doped complexes as calculated from luminescence spectra at 10 K (λ_{exc}: $^5D_0 \leftarrow {}^7F_0$).

Level	**9**	I_{rel}(**9**)	**5**	I_{rel}(**5**)	Gd(2% Eu) **6a**	I_{rel}	La(2% Eu) **1a**	I_{rel}	Lu(2% Eu) **3a**, I_{rel}
$^7F_0$ (λ_{exc}) [a]	17216		17219		17217		17246		17211
$^7F_1$	307	1.00	336	1.00	334	1.00	331	1.00	1.00
	399		360		362		349		
	419		417		414		432		
$^7F_2$	968	4.42	951	4.66	951	5.44	957	1.72	3.5
	983		992		990		987		
	1062		1018		1040		1011		
	1133		1040				1170		
$^7F_3$	1829	0.05	1831	[b]	[b]	[b]	1849	[b]	[b]
$^7F_4$	2641	1.32	2665	1.11	2664	1.37	2695	1.34	0.9
	2818		2834		2832		2803		
	2829		2872		2871		2915		
							3007		

[a] Energy of the $^5D_0 \leftarrow {}^7F_0$ transition (given in cm^{-1}) used as λ_{exc} for the laser-excited emission spectra. [b] Too weak to measure.

0947-6539/97/0310-1650 $ 17.50+.50/0 *Chem. Eur. J.* **1997**, *3*, No. 10

related geometry.[18, 25] Frey and Horrocks have recently proposed a correlation between the energy of the $^5D_0 \leftarrow {}^7F_0$ transition ($\tilde{\nu}$) and parameters describing the ability δ_i of n_i coordinating atoms i to produce a nephelauxetic effect [Eq. (1)].[40] A simple calculation for Eu^{III} in **9** using $C_{CN} = 1.0$ (coefficients

$$\tilde{\nu} = \tilde{\nu}_0 + C_{CN} \sum_i n_i \delta_i \quad (1)$$

for nonacoordination),[40] $\tilde{\nu}_0 = 17374\ cm^{-1}$,[40] $\delta_{N-heterocyclic} = -15.3$,[22, 25] and $\delta_{O-carboxamide} = -15.7$[40] predicts an energy of 17233 cm^{-1} for the $^5D_0 \leftarrow {}^7F_0$ transition at 295 K in qualitatively good agreement with the observed transition at 17227 cm^{-1} (fwhh = 9.5 cm^{-1} at 295 K).

The emission spectrum obtained through selective laser excitation at the maximum of the $^5D_0 \leftarrow {}^7F_0$ transition (17216 cm^{-1} at 10 K, fwhh = 2.4 cm^{-1}) provides a $^5D_0 \rightarrow {}^7F_J$ ($J = 1-4$) pattern typical for Eu^{III} in a pseudo-trigonal coordination site (Figure 4).[17, 18] The magnetic dipole $^5D_0 \rightarrow {}^7F_1$ transition is split

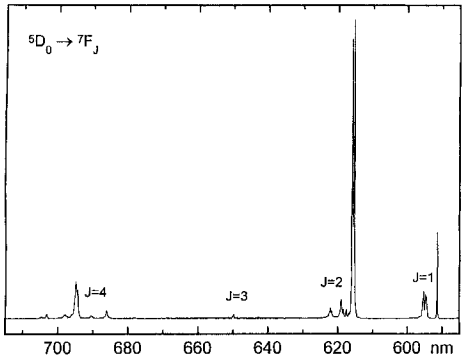

Figure 4. Part of the laser-excited emission spectrum of single crystals of $[Eu(L^9)_3](TfO)_3 \cdot 2THF$ (**9**) at 10 K (λ_{exc} = 580.86 nm). Vertical scale: arbitrary units.

into two main transitions $A_1 \rightarrow A_2$ and $A_1 \rightarrow E$ (both allowed in C_3, D_3, and D_{3h} symmetries); the latter are further split into two components separated by 20 cm^{-1} (Table 4) as similarly observed for $[Eu(L^1)_3](ClO_4)_3$ (15–18 cm^{-1})[17] and $[Eu(L^2)_3](ClO_4)_3$ (22 cm^{-1}).[18] The splitting arises from a slight deviation from the ideal trigonal symmetry and/or from a distortion induced by the excitation to the $^5D_0$ level, since the luminescence spectra reflect the properties of the excited state.[17, 18] The $^5D_0 \rightarrow {}^7F_2$ spectral region is dominated by two strong transitions, which we tentatively assign to the two allowed electric dipole $A_1 \rightarrow E$ transitions in D_3 as found for $[Eu(L^1)_3](ClO_4)_3$[17] and $[Eu(L^3)_3](ClO_4)_3$.[18] The small separation between these two transitions (15 cm^{-1}) may be interpreted as reflecting a site symmetry relatively close to D_{3h}. The observation of only three emission peaks in the region of the $^5D_0 \rightarrow {}^7F_4$ transition ($A_1' \rightarrow A_2''$, $2A_1' \rightarrow E''$) confirms the hypothesis of a slightly distorted D_{3h} microsymmetry around Eu^{III}, in agreement with the X-ray crystal structure of **9** (four and six allowed $^5D_0 \rightarrow {}^7F_4$ transitions are expected in D_3 and C_3 symmetries, respectively).[1]

The lifetime of the Eu($^5D_0$) level (Table 5) for **9** is long (1.7–1.8 ms) and reflects the absence of interaction with OH oscillators in the Eu^{III} coordination sphere.[1] The fact that it is unaffected by temperature variations (10–295 K) points to rather

Table 5. Observed lifetimes (τ, ms) of the Eu($^5D_0$) level in $[Eu(L^9)_3](TfO)_3 \cdot 2THF$ (**9**), $[Eu(L^9)_3](TfO)_3 \cdot H_2O$ (**5**), and 2% Eu-doped complexes at various temperatures in the solid state and in degassed acetonitrile solution.

Compd	λ_{exc} (cm^{-1})	10 K	77 K	295 K	295 K (sol.)
9	17218	1.78(3)	1.71(5)	1.80(4)	
	32468	1.79(3)	1.80(4)	1.71(11)	
5	17222	1.83(5)	1.90(3)	1.80(3)	2.49(16)
	32468	1.92(3)	1.93(3)	–	
Gd(2% Eu), **6a**	17227	1.79(7)	1.75(8)	1.66(7)	
	32468	1.89(7)	–	–	
Lu(2% Eu), **3a**	32468	1.6(2)	[a]	[a]	
La(2% Eu), **1a**	17256	0.79(2)	0.77(3)	0.66(1)	
	32468	0.77(2)	0.74(2)	0.52(9)	

[a] Too weak to measure.

inefficient vibrational quenching processes of the Eu($^5D_0$) level by the ligand backbone. Upon drying, crystals of **9** are transformed into a microcrystalline powder corresponding to complex **5** where the two THF molecules are replaced by one water molecule. The $^5D_0 \leftarrow {}^7F_0$ excitation spectrum consists of two distinct bands at 17219 cm^{-1} (fwhh = 3 cm^{-1}) and 17215 cm^{-1} (fwhh $\approx$ 9 cm^{-1}), suggesting the existence of at least two slightly different coordination sites in **5**. Excitation through these two components of the 0–0 transition yields very similar emission spectra. The $^5D_0 \rightarrow {}^7F_J$ ($J = 1-4$) pattern in the emission spectrum of **5** is different from that observed for **9**; this reflects a change in the symmetry of the Eu^{III} coordination site (cf. the splitting of the $^7F_1$ level, Table 4). However, the fact that the Eu($^5D_0$) lifetime remains long for **5** indicates that the water molecule does not enter the first coordination sphere. A similar situation has been observed in the dinuclear triple helicate $[Eu_2(L^5)_3](MeCN)_9(ClO_4)_6$.[21] The introduction of small amount of Eu^{III} (2%) into the La (**1a**), Gd (**6a**), and Lu (**3a**) complexes provides a means to probe the coordination site around the metal ions.[1] The emission spectra together with the measured lifetimes of both 2% Eu-doped complexes **3a** and **6a** are similar to those found for **5** and point to isostructural nonacoordinate complexes for the complete series Eu–Lu (Tables 4 and 5, Figure F1 in the Supporting Information). However, the lifetime is significantly reduced for the 2% Eu-doped La complex **1a**; this strongly suggests some close interaction between Eu^{III} and a water molecule in this compound.[2, 41] Moreover, the relative intensity of the $^5D_0 \rightarrow {}^7F_2$ transition is reduced with respect to **3a** and **6a**, and the $^5D_0 \leftarrow {}^7F_0$ transition is red-shifted by 27 cm^{-1} at 10 K, reflecting a higher coordination number than in **3a**, **5**, or **6a**. Although elemental analysis suggests that **1** is anhydrous, the IR spectrum of **1a** clearly indicates that this compound contains water. A rough estimation using the empirical equation of Horrocks and Sudnick [Eq. (2)],[41] with

$$q = A_{Eu}(\tau_{H_2O}^{-1} - \tau_{D_2O}^{-1}) \quad (2)$$

$A_{Eu} = 1.05$ and $\tau_{D_2O} = 1.8$ ms (the lifetime of Eu^{III} in **9** where no water molecule is bound to the metal), predicts that the coordination of one water molecule to Eu^{III} ($q = 1.0$) in this environment reduces the lifetime of the Eu($^5D_0$) level to 0.66 ms, a value identical with the observed lifetime at 295 K (Table 5).

We conclude from the photophysical studies that Eu^{III} lies in a fairly well-protected pseudo-D_{3h} coordination site in **9**, in agreement with its crystal structure. However, the crystalline

  0947-6539/97/0310-1651 $ 17.50+.50/0

edifice is very sensitive to the loss of interstitial solvent molecules, and the replacement of the THF molecules in **9** with one water molecule in **5** strongly alters the crystallinity of the sample leading to the existence of several slightly different coordination sites of lower symmetry. Luminescence from 2% Eu-doped complexes show that the Gd^{III} and the Lu^{III} complexes are isostructural with **5**, but the emission properties of Eu^{III} in the 2% Eu-doped La complex **1a** point to a different chemical arrangement around Eu^{III} involving the coordination of one water molecule. This result is in line with the distortion observed in the crystal structure of the La complex **8**, where the bound pyridine rings are severely tilted to accommodate the larger La^{III} in the cavity leading to a reduced protection of the metallic coordination site.

Behavior and structure of $[Ln(L^9)_3]^{3+}$ (Ln = La to Lu) in acetonitrile solution: A reliable qualitative analysis of the complexes formed in solution is obtained by electrospray MS (ES-MS) titrations of 10^{-4} M acetonitrile solutions of L^9 with $Ln(TfO)_3 \cdot nH_2O$ (Ln = La, Ce, Pr, Nd, Sm). As expected, we observe the successive formation of the three complexes $[Ln(L^9)_i]^{3+}$ ($i = 1-3$) together with their adducts with triflate anions (Figure 5, Table S1 Supporting Information).[42] As a result of the large solvation energies of Ln^{III},[43] associated with variable ES-MS responses for lanthanide complexes[44] and the strong ES-MS response of traces of protonated ligand ($[L^9+H]^+$, $m/z = 278.1$),[22, 25] a quantitative interpretation of the ES-MS peaks is not possible,[22, 44] but the evolution of the spectra during the titration clearly establishes that significant amounts of $[Ln(L^9)_2]^{3+}$ and $[Ln(L^9)_3]^{3+}$ coexist in solution for a stoichiometric ratio $Ln:L^9 = 1:3$ and a total ligand concentration of 10^{-4} M. This result suggests that the 1:3 complexes have a limited stability in solution. A careful examination of the spectra for $Ln:L^9 = 1:3$ (Ln = La, Ce, Pr, Nd) shows the existence of weak ES-MS peaks corresponding to traces of unexpected 1:4 complexes $[Ln(L^9)_4]^{3+}$ and $[Ln(L^9)_4(TfO)]^{2+}$. ES-MS spectra recorded under the same conditions indicate that the intensity of the peak corresponding to $[Ln(L^9)_4]^{3+}$ decreases stepwise on going from La^{III} to Pr^{III}; the signal for Nd^{III} is faint and completely disappears for Sm^{III}. The formation of $[Ln(L^9)_4]^{3+}$ in solution is thus closely related to the size of Ln^{III} and the accessibility of the metallic site in $[Ln(L^9)_3]^{3+}$ for further complexation. This implies that large Ln^{III} ions are less efficiently protected from external interactions in $[Ln(L^9)_3]^{3+}$, in agreement with the solid-state photophysical investigations. Tandem MS–MS experiments at low collision energy (30 eV) show that $[Ln(L^9)_4]^{3+}$ is weakly stable in the gas phase and readily fragments to give quantitatively $[Ln(L^9)_3]^{3+}$.

Upon complexation to Ln^{III}, the absorption spectrum of L^9 is significantly modified both in shape and intensity (Table 3). This allows a quantitative analysis of the complexation process by means of spectrophotometric titrations. Spectrophotometric data obtained under the same conditions as those described for ES-MS (total ligand concentration 10^{-4} M) and for $Ln:L^9$ ratios in the range 0.1–2.0 (Ln = La to Lu) display one pronounced end point for $Ln:L^9 = 0.33$ followed by a smooth evolution until $Ln:L^9 = 1.0-1.1$. Factor analysis[45] points to four absorbing species and the data can be fitted satisfactorily to Equations (3–5) (Table 6, Figure 6).

$$Ln^{3+} + L^9 \rightleftharpoons [Ln(L^9)]^{3+} \quad \log(\beta_1^{Ln}) \tag{3}$$

$$Ln^{3+} + 2L^9 \rightleftharpoons [Ln(L^9)_2]^{3+} \quad \log(\beta_2^{Ln}) \tag{4}$$

$$Ln^{3+} + 3L^9 \rightleftharpoons [Ln(L^9)_3]^{3+} \quad \log(\beta_3^{Ln}) \tag{5}$$

Strongly correlated calculated UV spectra are obtained for the various complexes $[Ln(L^9)_i]^{3+}$ ($i = 1-3$), leading to large uncertainties for the stability constants. Attempts to fit the data with a supplementary species $[Ln(L^9)_4]^{3+}$ failed because 1) only a minor amount of this complex is expected in solution according to the ES-MS titrations and 2) the UV spectra of the various complexes are too similar to allow the introduction of a fourth absorbing complex in the model. The values of $\log(\beta_3^{Ln})$ for Ln = La to Lu increase smoothly with decreasing Ln^{III} ionic radius (R^i),[38] and a plot of $\log(\beta_3^{Ln})$ vs. $1/R^i$ is roughly linear and corresponds to the classical electrostatic behavior[8, 14] associated with the increase of the charge density on Ln^{III} on going from

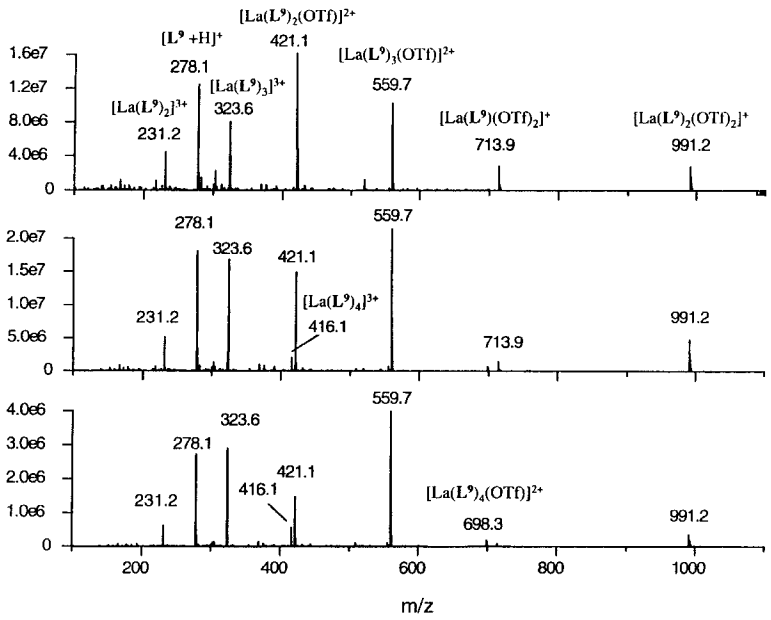

Figure 5. ES-MS titration of L^9 (10^{-4} M) with $La(TfO)_3 \cdot 3H_2O$ in acetonitrile for ratios $La:L^9 = 1:1$ (top), $La:L^9 = 1:2$ (middle), and $La:L^9 = 1:3$ (bottom).

Table 6. Cumulative stability constants ($\log(\beta_i^{Ln})$) for the complexes $[Ln(L^9)_i]^{3+}$ ($i = 1-3$) in acetonitrile at 25 °C.

Metal	$\log(\beta_1)$	$\log(\beta_2)$	$\log(\beta_3)$	Metal	$\log(\beta_1)$	$\log(\beta_2)$	$\log(\beta_3)$
La^{III}	7.4(3)	14.8(3)	21.0(3)	Dy^{III}	7.5(3)	14.8(4)	22.5(4)
Ce^{III}	7.6(3)	14.3(4)	22.0(3)	Ho^{III}	7.3(4)	14.8(4)	22.3(4)
Pr^{III}	7.6(3)	14.6(3)	22.2(3)	Er^{III}	7.7(4)	14.4(4)	22.7(4)
Nd^{III}	7.5(3)	13.8(4)	21.5(4)	Tm^{III}	8.5(3)	16.0(3)	22.1(4)
Sm^{III}	7.3(3)	14.4(4)	22.0(4)	Yb^{III}	8.5(3)	15.6(3)	22.8(4)
Eu^{III}	8.3(3)	15.3(3)	22.3(3)	Lu^{III}	8.1(3)	15.2(3)	22.9(3)
Gd^{III}	7.9(3)	14.7(4)	22.6(4)	Y^{III}	7.6(3)	14.6(4)	22.4(4)
Tb^{III}	8.2(3)	14.5(4)	22.9(4)				

0947-6539/97/0310-1652 $ 17.50+.50/0 Chem. Eur. J. 1997, 3, No. 10

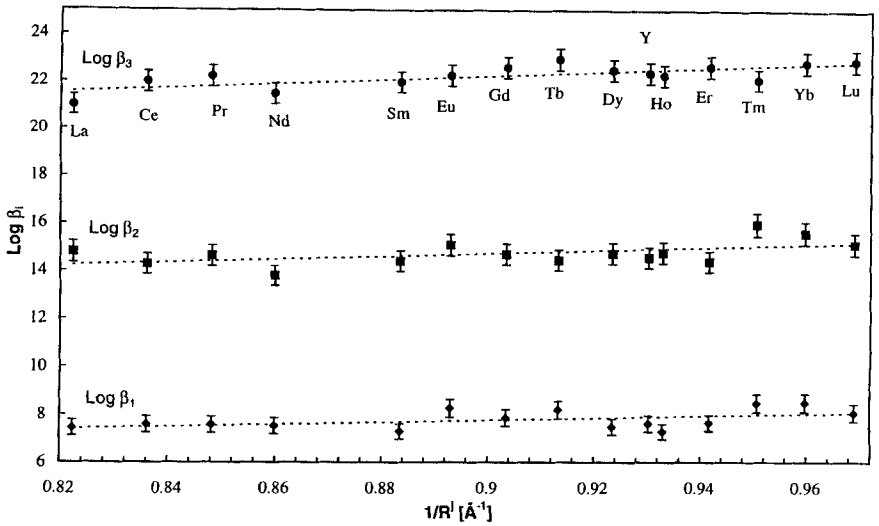

Figure 6. Stability constants $\log(\beta_i^{Ln})$ for $[Ln(\mathbf{L}^9)_i]^{3+}$ (i = 1–3) *vs* $1/R^i$ (R^i ionic radii of nine coordinate Ln^{III}).[38]

La to Lu, as has been similarly observed for $[Ln(\mathbf{L}^{10} - 2H)_3]^{3-}$ in water (Ln = La–Dy).[26] This trend strongly contrasts with the sigmoïdal behavior observed for $[Ln(\mathbf{L}^1)_3]^{3+}$, which has been explained by means of interstrand interactions between the benzimidazole side arms.[17, 19]

The affinity of $\mathbf{L}^9$ for Eu^{II} can be assessed by means of electrochemistry.[46] The cyclic voltammogram of $[Eu(\mathbf{L}^9)_3]^{3+}$ in acetonitrile displays a quasi-reversible cathodic wave at $E_{1/2} = -0.62$ V vs. SCE, assigned to the Eu^{III}/Eu^{II} reduction process, together with three broad and irreversible ligand-centered reduction waves (−0.62, −1.30, and −1.38 V vs. SCE), which are similarly observed for $[Ln(\mathbf{L}^9)_3]^{3+}$ (Ln = Y, Lu). Taking into account the potential of solvated Eu^{III}/Eu^{II} in acetonitrile ($E_{1/2} = +0.21$ V vs. SCE),[47] we can estimate the ratio of the stability constants as shown in Equation (6). The large

$$\log\left(\frac{\beta_3^{Eu(II)}}{\beta_3^{Eu(III)}}\right) = \frac{1}{0.059}(E_{1/2}([Eu(\mathbf{L}^9)_3]^{3+}) - E_{1/2}(Eu^{3+})) = -13.4 \quad (6)$$

negative value obtained is identical to that found for $[EuFe(\mathbf{L}^7)_3]^{5+}$ [48] where Eu^{III} is coordinated by carboxamide side arms, which are known to destabilize Eu^{II}.[47, 48] From the $\log(\beta_3^{Eu(III)})$ value determined spectrophotometrically, $\log(\beta_3^{Eu(II)})$ is calculated to be approximately 9 for $[Eu(\mathbf{L}^9)_3]^{2+}$. Carboxamide groups thus have a weaker affinity for Eu^{II} than benzimidazole groups, since $\log(\beta_3^{Eu(II)}) \approx 17$ for $[Eu(\mathbf{L}^1)_3]^{2+}$.[49]

The ^1H and ^{13}C NMR spectra were recorded in acetonitrile for a total ligand concentration of 0.15 M and for Ln:$\mathbf{L}^9$ = 0.33, so that the complexes $[Ln(\mathbf{L}^9)_3]^{3+}$ are predominant in solution (≥99% according to stability constants reported in Table 6). ^1H and ^{13}C NMR signals were assigned by using 2D $\{^1H-^1H\}$ COSY and 2D $\{^1H-^{13}C\}$ HETCOR NMR correlation spectroscopies and nuclear Overhauser effects (NOE; measured for 0.01 M solution; Table 7). The ^{13}C NMR spectrum of the diamagnetic complex $[La(\mathbf{L}^9)_3]^{3+}$ displays eight signals corresponding to three equivalent ligand strands related by a C_3 axis passing through the metal and three C_2 axes or a σ_h plane perpendicular to the C_3 axis leading to D_3 or D_{3h} symmetries, respectively, on the NMR timescale. The downfield shifts of C^2 and C^3 in $[La(\mathbf{L}^9)_3]^{3+}$ (+3.71 and +4.81 ppm, respectively, with respect to the free ligand; Table 7) are typical of N-coordinated pyridine rings.[50] To a lesser extent, the signal of the carbonyl C^4 is also shifted downfield (+1.52 ppm); this has been tentatively attributed to the coordination of the oxygen atom to Ln^{III}.[32] The observation of two well-resolved sets of signals for the methylenes $C^{5,7}$ and the methyls $C^{6,8}$ indicates that the rotation about the C^4–N(amide) bond is severely hindered in the complex as a consequence of the drainage of the electron density from the coordinated carbonyl group toward La^{III}.[32] The ^1H NMR spectrum of $[La(\mathbf{L}^9)_3]^{3+}$ confirms the N-coordination of the central pyridine ring in solution ($H^{2,3}$ are shifted downfield)[50] and the hindered rotation around the C^4–N bond (two quartets observed for $H^{5,5'}$ and $H^{7,7'}$), but the observation of enantiotopic protons for the methylenes $H^{5,5'}$ and $H^{7,7'}$ implies the existence of three σ_v planes, leading to an average pseudo-cylindrical D_{3h} symmetry for $[La(\mathbf{L}^9)_3]^{3+}$ as a result of a fast $P \rightleftharpoons M$ helical interconversion on the NMR timescale at room temperature. Addition of an excess of $\mathbf{L}^9$ to a solution of $[La(\mathbf{L}^9)_3]^{3+}$ does not give separate signals for free and coordinated $\mathbf{L}^9$, in agreement with the exis-

Table 7. NMR shifts (with respect to TMS) for ligand $\mathbf{L}^9$ and its complexes $[Ln(\mathbf{L}^9)_3]^{3+}$ in CD_3CN at 298 K.

a) ^1H NMR shifts.

Compd	H^2	H^3	$H^{5,5'}$	H^6	$H^{7,7'}$	H^8
$\mathbf{L}^9$	7.63	7.87	3.56	1.26	3.34	1.15
$[La(\mathbf{L}^9)_3]^{3+}$	7.94	8.30	3.56	1.31	3.32	1.01
$[Y(\mathbf{L}^9)_3]^{3+}$	8.06	8.34	3.69, 3.70	1.37	3.14, 3.30	0.88
$[Lu(\mathbf{L}^9)_3]^{3+}$	8.08	8.36	3.72, 3.72	1.39	3.11, 3.29	0.63
$[Ce(\mathbf{L}^9)_3]^{3+}$	9.13	9.61	3.65	1.45	3.36	0.63
$[Pr(\mathbf{L}^9)_3]^{3+}$	10.38	10.69	3.93	1.60	2.44	−0.40
$[Nd(\mathbf{L}^9)_3]^{3+}$	9.22	9.38	3.63	1.45	3.61	0.83
$[Sm(\mathbf{L}^9)_3]^{3+}$	8.15	8.47	3.66	1.35	3.22	0.83
$[Eu(\mathbf{L}^9)_3]^{3+}$	6.00	6.77	3.60	1.22	3.61, 3.98	1.48
$[Tb(\mathbf{L}^9)_3]^{3+}$	19.17	18.70	0.44, 4.83	1.17	−5.86, 0.35	−9.39
$[Er(\mathbf{L}^9)_3]^{3+}$	4.29	4.70	3.21, 4.70	1.14	5.85, 8.48	1.14
$[Tm(\mathbf{L}^9)_3]^{3+}$	4.31	4.89	4.56, 6.38	1.22	1.87, 3.56	2.06
$[Yb(\mathbf{L}^9)_3]^{3+}$	6.60	6.91	3.61, 4.40	1.20	3.10, 4.40	2.04

b) ^{13}C NMR shifts.

Compd	C^1	C^2	C^3	C^4	C^5	C^6	C^7	C^8
$\mathbf{L}^9$	153.47	123.55	137.85	167.97	43.17	14.15	40.07	12.71
$[La(\mathbf{L}^9)_3]^{3+}$	150.84	127.26	142.66	169.49	45.24	13.96	42.91	12.24
$[Y(\mathbf{L}^9)_3]^{3+}$	149.33	128.10	142.76	169.05	45.58	13.98	44.11	12.20
$[Lu(\mathbf{L}^9)_3]^{3+}$	153.97	132.88	142.78	168.69	45.96	13.75	43.73	11.70
$[Ce(\mathbf{L}^9)_3]^{3+}$	153.97	132.88	142.78	168.69	45.96	13.75	43.73	11.70
$[Pr(\mathbf{L}^9)_3]^{3+}$	159.04	142.39	141.65	170.99	47.06	13.51	43.61	10.68
$[Nd(\mathbf{L}^9)_3]^{3+}$	154.24	143.53	138.61	170.14	47.19	13.44	44.72	11.93
$[Sm(\mathbf{L}^9)_3]^{3+}$	151.84	127.42	143.23	171.97	45.51	14.05	43.65	12.18
$[Eu(\mathbf{L}^9)_3]^{3+}$	145.41	95.92	152.29	163.22	43.05	15.40	42.53	13.47
$[Tb(\mathbf{L}^9)_3]^{3+}$	186.77	66.71	194.32	135.42	35.83	10.64	35.32	10.64
$[Er(\mathbf{L}^9)_3]^{3+}$	129.76	88.91	152.92	137.94	47.39	17.66	42.41	10.56
$[Tm(\mathbf{L}^9)_3]^{3+}$	135.09	106.11	145.65	138.96	44.91	15.45	44.05	14.23
$[Yb(\mathbf{L}^9)_3]^{3+}$	140.61	121.172	143.09	153.83	45.31	14.43	44.94	13.74

  0947-6539/97/0310-1653 $ 17.50+.50/0

tence of a fast ligand exchange processes on the NMR timescale. The ^{1}H NMR spectra for $[Ln(\mathbf{L^9})_3]^{3+}$ (Ln = Y, Lu) are similar except for the dynamic processes occurring in solution. An excess of ligand produces distinct signals for free and coordinated $\mathbf{L^9}$ at room temperature, and the methylene proton pairs $H^{5,5'}$ and $H^{7,7'}$ are each diastereotopic (observed as pseudo-sextets[33]) pointing to a blocked D_3-symmetrical triple-helical structure. Coalescence of the two sextets assigned to H^5 and $H^{5'}$ to give the quartet expected for an average D_{3h} symmetry occurs at 318 K for $[Y(\mathbf{L^9})_3]^{3+}$ and 333 K for $[Lu(\mathbf{L^9})_3]^{3+}$. These results lead to estimated energy barriers $\Delta G(T_{coal})$ of 73 and 78 kJ mol^{-1} for the dynamic helical $P \rightleftharpoons M$ interconversion, according to a simplified treatment of the Eyring equation (Figure 7).[51] These data strongly suggest that small Ln^{III} ions produce kinetically inert D_3 triple-helical complexes $[Ln(\mathbf{L^9})_3]^{3+}$ on the NMR timescale, while larger Ln^{III} ions lead to average pseudo-cylindrical D_{3h} structures arising from fast $P \rightleftharpoons M$ interconversion. As expected, the transition between these two dynamic behaviors is gradual, and the variable-temperature NMR study of $[Sm(\mathbf{L^9})_3]^{3+}$ (the weak paramagnetism of Sm^{III} has only negligible influence on the line broadening)[52] shows that the diastereotopic protons $H^{7,7'}$ become enantiotopic at 263 K, which involves an energy barrier of only 55 kJ mol^{-1}.[51] For $[La(\mathbf{L^9})_3]^{3+}$, the signals of $H^{5,5'}$ and $H^{7,7'}$ remain enantiotopic at the lowest accessible temperature in acetonitrile (233 K), indicating an even smaller energy barrier.

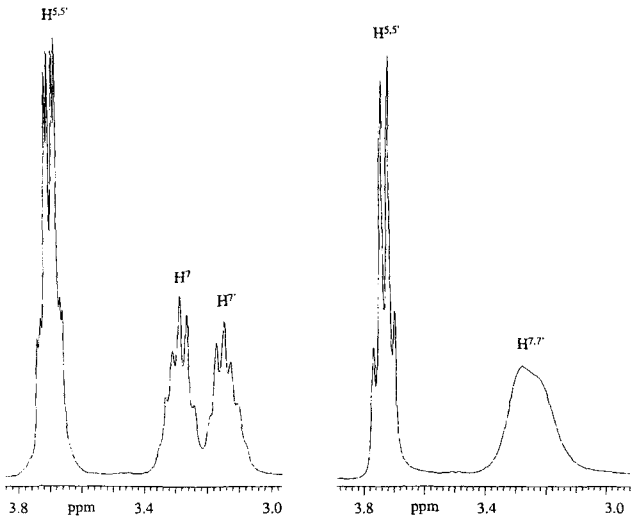

Figure 7. Part of the ^{1}H NMR spectra of $[Y(\mathbf{L^9})_3]^{3+}$ in CD_3CN showing the signals of the methylene protons $H^{5,5'}$ and $H^{7,7'}$ at 294 K (left) and 333 K (right).

Further structural information is gained from the use of paramagnetic Ln^{III} ions, which allow the separation of contact (δ_{ij}^{c}) and pseudo-contact (δ_{ij}^{pc}) contributions to the isotropic NMR paramagnetic shifts (δ_{ij}^{iso}).[25, 27, 52] A straightforward separation of a contact term F_i and a pseudo-contact term G_i for each nucleus i in the axial lanthanide complexes $[Ln(\mathbf{L^9})_3]^{3+}$ uses 1) Equation (7), 2) the theoretical values for $\langle S_z \rangle_j$ (the expectation value of S_z)[53] and C_j (the anisotropic part of the axial magnetic susceptibility tensor)[54] of the free ions, and 3) multilinear regression for at least two different paramagnetic Ln_j^{III}.[25, 27] The contact term F_i is given by Equation (8) and

$$\delta_{ij}^{iso} = \delta_{ij}^{exp} - \delta_i^{dia} = \delta_{ij}^{c} + \delta_{ij}^{pc} = F_i \langle S_z \rangle_j + G_i C_j \quad (7)$$

$$F_i = \frac{A_i}{\hbar \gamma B_0} \quad (8)$$

reflects through-bond Fermi interactions between the paramagnetic center and the nucleus i (A_i is the hyperfine interaction parameter and B_0 the applied magnetic induction).[53] The pseudo-contact term G_i depends on the geometric position of the nucleus i (r_i and θ_i are the internal axial coordinates of the nucleus i with respect to the ligand field axes) for a particular ligand field constant a at a given temperature T [Eq. (9)].[27, 54]

$$G_i = \frac{a}{T^2} \frac{1 - 3\cos^2\theta_i}{r_i^3} \quad (9)$$

The diamagnetic correction δ_i^{dia} in Equation (7) is taken from the chemical shifts measured for the isostructural diamagnetic complexes: $[La(\mathbf{L^9})_3]^{3+}$ for Ln = Ce–Nd, $[Y(\mathbf{L^9})_3]^{3+}$ for Ln = Sm–Dy, and $[Lu(\mathbf{L^9})_3]^{3+}$ for Ln = Ho–Yb.[55] This simple approach gives satisfactory results provided that the complexes $[Ln(\mathbf{L^9})_3]^{3+}$ are isostructural in solution. This must be checked graphically from plots of $\delta_{ij}^{iso}/\langle S_z \rangle_j$ vs. $C_j/\langle S_z \rangle_j$ [Eq. (10)] and δ_{ij}^{iso}/C_j vs. $\langle S_z \rangle_j/C_j$ [Eq. (11)], which are expected

$$\frac{\delta_{ij}^{iso}}{\langle S_z \rangle_j} = F_i + G_i \frac{C_j}{\langle S_z \rangle_j} \quad (10)$$

$$\frac{\delta_{ij}^{iso}}{C_j} = F_i \frac{\langle S_z \rangle_j}{C_j} + G_i \quad (11)$$

to be linear for isostructural series.[56] Analysis of the paramagnetic data of Table 7 for each measured nucleus i in $[Ln(\mathbf{L^9})_3]^{3+}$ according to Equations (10) and (11) systematically produces two straight lines associated with two different isostructural series involving respectively large Ln^{III} ions (Ce–Tb) and small Ln^{III} ions (Er–Yb) (Figure 8). A structural change thus occurs

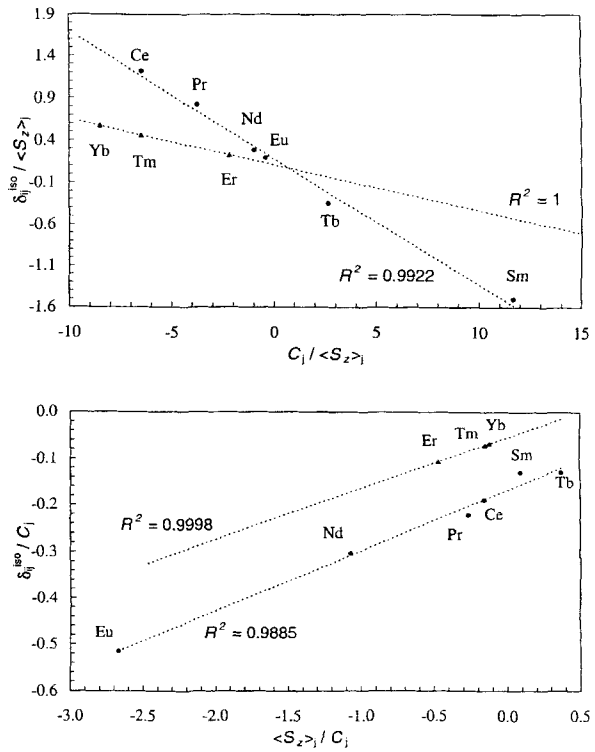

Figure 8. Plot for H^2 in $[Ln(\mathbf{L^9})_3]^{3+}$ at 298 K of $\delta_{ij}^{iso}/\langle S_z \rangle_j$ vs. $C_j/\langle S_z \rangle_j$ [Eq. (10)] (top) and δ_{ij}^{iso}/C_j vs. $\langle S_z \rangle_j/C_j$ [Eq. (11)] (bottom).

0947-6539/97/0310-1654 $ 17.50+.50/0 Chem. Eur. J. 1997, 3, No. 10

Table 8. Computed values for contact (F_i) and pseudo-contact (G_i) terms for ^1H and ^{13}C nuclei in paramagnetic complexes $[Ln(\mathbf{L^9})_3]^{3+}$ in CD_3CN at 298 K using Equation (7) [27].

a) Series Ln = Ce–Tb.

	H^2	H^3	H^6	H^8	C^1	C^2	C^3	C^4	C^5	C^6	C^7	C^8
F_i	0.129(4)	0.11(1)	0.023(7)	0.00(2)	0.25(9)	3.01(9)	−1.02(3)	0.6(1)	0.31(5)	−0.07(3)	0.23(5)	−0.11(3)
G_i	−0.177(2)	−0.160(5)	−0.006(3)	0.118(6)	−0.53(4)	−0.40(3)	−0.22(1)	0.16(5)	0.00(2)	0.064(9)	0.02(2)	0.06(1)
AF_i	0.01	0.04	0.49	0.05	0.07	0.04	0.02	0.11	0.13	0.20	0.16	0.31

b) Series Ln = Er–Yb

	H^2	H^3	H^6	H^8	C^1	C^2	C^3	C^4	C^5	C^6	C^7	C^8
F_i	0.110(1)	0.14(1)	0.01(1)	−0.26(9)	0.9(4)	2.495(1)	−0.82(2)	1.1(4)	−0.21(2)	−0.267(4)	0.19(6)	0.30(4)
G_i	−0.054(1)	−0.044(4)	−0.003(4)	−0.01(3)	−0.14(9)	−0.034(1)	−0.072(1)	−0.4(1)	−0.045(4)	−0.014(1)	0.03(2)	0.09(1)
AF_i	0.00	0.02	0.33	0.20	0.13	0.00	0.01	0.08	0.06	0.01	0.24	0.13

between Tb and Er in solution, in agreement with the solid-state investigation. We cannot distinguish whether this change is gradual or abrupt for a particular ionic radius since the increased nuclear relaxation induced by Dy^{III} and Ho^{III}[52] prevents a complete and reliable assignment of the various signals in the NMR spectra of $[Ln(\mathbf{L^9})_3]^{3+}$ (Ln = Dy, Ho), and these metal ions have been excluded from the fitting process. The complete paramagnetic data of Table 7 can be fitted to Equation (7) based on two different isostructural series (Ln = La–Tb and Er–Yb), and the resulting F_i, G_i terms and agreement factors AF_i[25, 27] are collected in Table 8 (the computed corrected contact and dipolar contributions are given as Supporting Information, Table S2). The diastereotopic methylene protons $H^{5,5'}$ and $H^{7,7'}$ have been omitted from the fitting process since no reliable assignment is possible for the separated signals of the ABX_3 spin system.[25]

The agreement factors AF_i are large ($0.01 < AF_i < 0.49$) compared to those obtained for $[Ln(\mathbf{L^{10}} - 2H)_3]^{3-}$ ($0.04 < AF_i < 0.27$),[27] but still satisfactory for both isostructural series when we exclude H^6 ($0.01 < AF_i < 0.31$), which has negligible induced paramagnetic shifts (Table 7). The sizable F_i values of H^2 (0.13, 0.11) and H^3 (0.11, 0.14) demonstrate a significant spin delocalization onto the coordinated pyridine rings, which can be compared to those found for $[Ln(\mathbf{L^{10}} - 2H)_3]^{3-}$ (0.009 and 0.013, respectively)[27], $[LnZn(\mathbf{L^7})_3]^{5+}$ (0.22 and 0.17, respectively)[25] and $[LnZn(\mathbf{L^6})_3]^{5+}$ (0.34 and 0.18, respectively).[22] The *N*,*N*′-diethylcarbamoyl groups bound to the 2,6-positions of the coordinated pyridine ring in $\mathbf{L^9}$ thus induce a delocalization of the spin density onto the central aromatic ring that is intermediate between the negatively charged carboxylate groups of $[\mathbf{L^{10}} - 2H]^{2-}$ and the aromatic benzimidazole side arms in $\mathbf{L^6}$. In contrast, the F_i values found for C^4 (1.12 for both series) are similar to those found for $[Ln(\mathbf{L^{10}} - 2H)_3]^{3-}$ (1.28);[27] this indicates that the delocalization onto the carbonyl groups is comparable for coordinated carboxylate and carboxamide side arms. The G_i values are difficult to correlate to the atomic position of the nucleus *i* since they depend on the two axial coordinates θ_i and r_i. However, the particular angular position of C^3 and H^3 ($\theta_3 = \pi/2$) can be used as NMR structural probes for both series. The G_3 values of H^3 and C^3 in $[Ln(\mathbf{L^9})_3]^{3+}$ are negative (Table 8) and are significantly reduced for the second series (Ln = Er–Yb). These results can tentatively be explained in terms of an increase in the Ln–C^3 (or Ln–H^3) distances r_3, implying a flattening of the triple-helical structure along the C_3 axis in solution. This statement is confirmed by the variation of the G_4 values of C^4, which are positive for Ln = Ce–Tb ($G_4 = 0.16$, $\theta_4 < 54.7°$) and negative for Ln = Er–Yb ($G_4 = -0.42$, $\theta_4 > 54.7°$).

We conclude from the NMR studies that both isostructural series adopt a triple-helical structure in solution. For the large cations (La–Tb), an average pseudo-cylindrical D_{3h}-symmetrical structure is observed at room temperature on the NMR timescale, which results from fast helical interconversion. For the small ions (Er–Lu), a more compact and dynamically blocked D_3-symmetrical structure flattened along the C_3 axis is observed on the NMR timescale. An improved method for the separation of contact and pseudo-contact shift in paramagnetic Ln^{III} complexes has been developed by Kemple et al.[55] Starting from known axial coordinates θ_i and r_i for each nucleus (taken from molecular mechanics or X-ray crystal structures), a multilinear least-squares fitting of Equation (12) allows the simultaneous calculation of 1) the experimental axial anisotropic susceptibility parameter $\xi\chi_j^{zz}$ and 2) the contact contributions δ_{ij}^c.[25] Using the C_3 average internal axial coordinates θ_i and r_i calculated from the crystal structure of $[Eu(\mathbf{L^9})_3](TfO)_3 \cdot 2THF$ (**9**) (the Eu atom is placed at the origin, and the *z* axis corresponds to the pseudo-C_3 axis),[25] the experimental paramagnetic isotropic shifts (δ_{ij}^{iso}) are fitted to Equation (12) with nine parameters for each lanthanide *j* (10×9 fits; $\xi\chi_j^{zz}$, δ_C1-5^c, δ_C7^c, δ_H2-3^c; Table S3 in the Supporting Information).[55] Contact contributions are neglected for the methyl groups C^6 and C^8, which are sufficiently remote from Ln^{III}. As expected from the increase of adjustable parameters used in this method, the agreement factors AF_i are improved ($0.00 < AF_i < 0.07$ except for C^6), but the average calculated F_i and G_i terms [Eqs. (7–9), Table S4][25] are very similar to those obtained directly from Equation (7) for the large cations (Ln = Ce–Tb); this indicates that the crystal structure of $[Eu(\mathbf{L^9})_3]^{3+}$ is a good model for the structure of $[Ln(\mathbf{L^9})_3]^{3+}$ (Ln = La–Tb) in solution. For the heavier Ln^{III} ions (Ln = Er, Yb), significant discrepancies between the G_i terms calculated with the two methods confirm that 1) a structural change occurs between Tb and Er and

$$\delta_{ij}^{iso} = \xi\chi_j^{zz}\frac{1-3\cos^2\theta_i}{r_i^3} + \sum_i \delta_{ij}^c \qquad (12)$$

  0947-6539/97/0310-1655 $ 17.50+.50/0

2) $[Ln(\mathbf{L}^9)_3]^{3+}$ (Ln = Er–Yb) adopts a more compact structure in solution than the model compound $[Eu(\mathbf{L}^9)_3]^{3+}$.

Finally, we have applied a simplified form of the Solomon–Bloembergen–Morgan equation[56, 57] for the estimation of Ln–C^i and Ln–H^i distances in $[Ln(\mathbf{L}^9)_3]^{3+}$. Assuming a pure paramagnetic dipolar relaxation mechanism Equation (13)

$$r_i = r_{ref}\left(\frac{T_{1c}^i}{T_{1c}^{ref}}\right)^{1/6} \quad (13)$$

holds,[57] where r_i is the Ln–nucleus$_i$ distance, r_{ref} is a reference distance (taken as the C_3 average distance of the nucleus with the largest distance from the Ln^{III} center),[57] and T_{1c}^i and T_{1c}^{ref} are the longitudinal relaxation times corrected for diamagnetic relaxation [Eq. (14)]; T_{1dia}^i are the relaxation times measured

$$\frac{1}{T_{1c}^i} = \frac{1}{T_1^i} - \frac{1}{T_{1dia}^i} \quad (14)$$

for the diamagnetic complexes $[Ln(\mathbf{L}^9)_3]^{3+}$ (Ln = La, Lu)). Table 9 reports the r_i distances calculated with the Ln–C^6 and Ln–H^3 distances taken from the X-ray crystal structure of **9** as references. For $[Eu(\mathbf{L}^9)_3]^{3+}$, we observe large discrepancies between distances found in the crystal structure of **9** and those estimated from Equation (13) in solution, since Eu^{III} induces a large contact contribution as a result of its large $\langle S_z \rangle$ coefficient,[53] and Equation (13) is thus no longer suitable. In contrast, Ce and Yb maximize the dipolar contributions[56] leading to estimated distances that are qualitatively in good agreement with those found in the crystal structure of **9**. Of particular interest is the variation of the ratio Ln–C^1/Ln–C^3, which reflects the average tilt of the pyridine ring on the NMR timescale. It amounts to 1.56 for $[Yb(\mathbf{L}^9)_3]^{3+}$ and only 1.32 for $[Ce(\mathbf{L}^9)_3]^{3+}$ in acetonitrile, strongly suggesting that the pyridine ring is more tilted (on average) for large Ln^{III} cations, in qualitative agreement with the crystal structure of $[La(\mathbf{L}^9)_3]^{3+}$.

Table 9. Estimated Ln–X^i distances for $[Ln(\mathbf{L}^9)_3]^{3+}$ in CD_3CN at 298 K from T_1 measurements and Equation (13).

Ln	C^1	C^2	C^3	C^4	C^5	C^6(ref)	C^7	C^8	H^2	H^3(ref)
Ce	3.61	4.28	4.75	3.45	5.58	6.76	4.84	5.29	5.50	6.26
Eu	3.68	4.92	4.49	3.41	4.89	6.76	4.52	6.28	5.56	6.26
Yb	3.65	4.96	5.68	3.50	6.39	6.76	5.29	5.73	5.47	6.26
9 [a]	3.41	4.72	5.24	3.27	5.62	6.76	4.96	5.19	5.53	6.26

[a] C_3 average distances calculated from the X-ray crystal structure of **9**.

Photophysical properties of $[Ln(\mathbf{L}^9)_3]^{3+}$ (Ln = La, Gd, Eu, Tb) in acetonitrile solution: The absorption spectra of $[Ln(\mathbf{L}^9)_3]^{3+}$ are similar for all studied Ln^{III} ions (Table 3) and show broad and intense bands in the UV region (35000–47000 cm^{-1}). The ligand-centered emission, observed as a faint signal in the solid state at 77 K, cannot be detected for $[Ln(\mathbf{L}^9)_3]^{3+}$ (Ln = La, Gd) in acetonitrile at room temperature, but $[Ln(\mathbf{L}^9)_3]^{3+}$ (Ln = Eu, Tb) display significant metal-centered luminescence upon irradiation into the ligand excited states, confirming the efficient $\mathbf{L}^9 \rightarrow Ln^{III}$ energy transfers previously exemplified in the solid state. The excitation spectra of $[Ln(\mathbf{L}^9)_3]^{3+}$ (Ln = Eu, Tb) display only a weak and broad peak centered at 32150 cm^{-1} for Eu and 31050 cm^{-1} Tb. This peak is located on the low-energy tail of the absorption spectra; this indicates that $\mathbf{L}^9$ is a poor sensitizer of Eu and Tb luminescence. The emission spectrum of $[Eu(\mathbf{L}^9)_3]^{3+}$ obtained upon direct irradiation of the Eu($^5L_6$) level (25188 cm^{-1}) is similar to that measured for the solid-state sample: the overall shape and the relative intensities of the $^5D_0 \rightarrow {}^7F_j$ transitions match those of complex **5** (Figure 9, Table S5 in the Supporting Information). Although the widths of the emission bands prevent site-symmetry analysis in solution, there is no doubt that the pseudo-trigonal triple-helical structure is maintained for $[Eu(\mathbf{L}^9)_3]^{3+}$ in acetonitrile (10^{-3} M) in agreement with NMR studies.

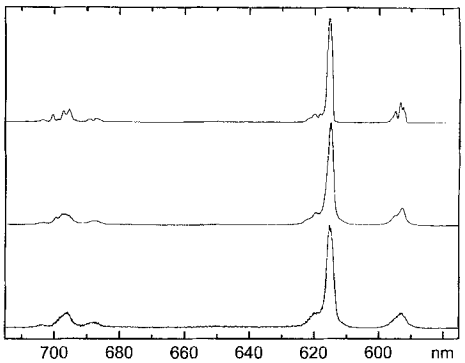

Figure 9. Emission spectra of complex **5** in the solid state: 10 K (top), 295 K (middle), and in acetonitrile solution (10^{-3} M, 295 K; bottom).

The Eu($^5D_0$) lifetime is longer than in the solid state pointing to negligible interactions of the solvent molecules in the first coordination sphere (Table 10). However, the quantum yield of $[Eu(\mathbf{L}^9)_3]^{3+}$ (10^{-3} M in acetonitrile) relative to $[Eu(terpy)_3]^{3+}$ is small ($\Phi_{rel} = 6.6\ 10^{-3}$; Table 10) and is intermediate between those reported for $[Eu(\mathbf{L}^1)_3]^{3+}$ ($\Phi_{rel} = 6.3 \times 10^{-5}$)[18] and $[EuZn(\mathbf{L}^7)_3]^{5+}$ ($\Phi_{rel} = 0.13$).[25] The extremely low quantum yield of $[Eu(\mathbf{L}^1)_3]^{3+}$ results from interstrand stacking interactions between the benzimidazole side arms,[17, 58] which are removed in the 1:1 complex $[Eu(\mathbf{L}^1)(NO_3)_3]$ leading to strongly luminescent stains ($\Phi_{rel} = 2.16$).[58] Despite similar triple-helical structure in $[Eu(\mathbf{L}^9)_3]^{3+}$ the carboxamide side arms do not exhibit significant interstrand interactions, and the 1:1 complex $[Eu(\mathbf{L}^9)(NO_3)_3]$ (**10**) is only slightly more luminescent in acetonitrile (Table 10). We thus conclude that the weak emission properties of $[Eu(\mathbf{L}^9)_3]^{3+}$ are associated with the limited antenna effect produced by the coordinated ligands $\mathbf{L}^9$. However, carboxamide groups are not alone responsible for this defect, since identical *N*,*N*′-diethylcarbamoyl groups coordinated to nonacoordinate Eu^{III} in $[EuZn(\mathbf{L}^7)_3]^{5+}$ produce strong luminescence.[25] Addition of water to a 10^{-3} M solution of $[Eu(\mathbf{L}^9)_3]^{3+}$ in anhydrous acetonitrile results in the simultaneous decrease of the quantum yield and Eu($^5D_0$) lifetime; this result points to inner sphere interactions of water molecules with Eu^{III}, probably associated with partial decomplexation of the ligand strands.

The quantum yield of $[Tb(\mathbf{L}^9)_3]^{3+}$ relative to $[Tb(terpy)_3]^{3+}$ is more promising. Addition of water produces similar, but less pronounced effects than those observed for $[Eu(\mathbf{L}^9)_3]^{3+}$, on the relative quantum yield and lifetime of the Tb($^5D_4$) level, in

0947-6539/97/0310-1656 $ 17.50+.50/0 Chem. Eur. J. 1997, 3, No. 10

Table 10. Quantum yields (Φ_{rel}) Relative to $[Eu(terpy)_3]^{3+}$ and $[Tb(terpy)_3]^{3+}$ (terpy = 2,2′:6′,2″-terpyridine) and lifetimes (τ) of the $Eu(^5D_0)$ and $Tb(^5D_4)$ levels for $[Ln(\mathbf{L^9})_3]^{3+}$ (Ln = Eu, Tb) in anhydrous acetonitrile at 298 K [a].

Compd	Conc. [b]	Added H_2O (M)	λ_{exc} (nm)	ε_{exc} ($M^{-1}cm^{-1}$)	Φ [c]	τ (ms)
$[Eu(terpy)_3]^{3+}$	10^{-3}	0	371	549	1.0	–
$[Eu(\mathbf{L^9})_3]^{3+}$	10^{-3}	0	312	569	6.6×10^{-3}	2.42(4)
$[Eu(\mathbf{L^9})_3]^{3+}$	10^{-3}	0.5	309	887	3.3×10^{-3}	1.64(6)
$[Eu(\mathbf{L^9})_3]^{3+}$	10^{-3}	1.0	310	708	4.1×10^{-3}	1.01(3)
$[Eu(\mathbf{L^9})_3]^{3+}$	10^{-4}	0	301	2904	1.0×10^{-3}	2.36(6)
$[Eu(\mathbf{L^9})(NO_3)_3]$	10^{-3}	0	309	369	2.7×10^{-2}	1.73(3)
$[Tb(terpy)_3]^{3+}$	10^{-3}	0	364	685	1.0	–
$[Tb(\mathbf{L^9})_3]^{3+}$	10^{-3}	0	322	185	0.74	1.85(3)
$[Tb(\mathbf{L^9})_3]^{3+}$	10^{-3}	0.5	320	222	0.55	1.75(3)
$[Tb(\mathbf{L^9})_3]^{3+}$	10^{-3}	1.0	319	235	0.47	1.62(3)
$[Tb(\mathbf{L^9})_3]^{3+}$	10^{-4}	0	298	626	0.1	1.85(3)
$[Tb(\mathbf{L^9})(NO_3)_3]$	10^{-3}	0	310	341	0.14	1.91(7)

[a] The quantum yields of $[Ln(terpy)_3]^{3+}$ relative to an aerated water solution of $[Ru(bipy)_3]^{2+}$ are 0.47 for Ln = Eu and 1.7 for Ln = Tb; these values allow the calculation of absolute quantum yields [59]. [b] Quantum yields are determined for 10^{-3} M solution to avoid decomplexation; values at 10^{-4} M are given for comparison. [c] Relative errors on Φ_{rel} are typically 10–15%.

agreement with the expected reduced quenching effect of water molecules for Tb^{III}.[41] As previously observed for Eu, the 1:1 complex $[Tb(\mathbf{L^9})(NO_3)_3]$ (**11**) displays a comparable quantum yield in acetonitrile confirming that the triple helical structure of $[Ln(\mathbf{L^9})_3]^{3+}$ is not responsible for extra nonradiative quenching processes.

Conclusions

Ligands $\mathbf{L^9}$ and $[\mathbf{L^{10}}-2H]^{2-}$ possess common structural features and binding abilities which have led to the erroneous conclusion that carboxylate and carboxamide side arms bound to the central pyridine ring provide triple-helical complexes $[Ln(\mathbf{L^9})_3]^{3+}$ with similar properties.[32] The molecular structures of $[Ln(\mathbf{L^9})_3]^{3+}$ (Ln = La, Eu) together with photophysical data suggest that the simultaneous coordination of the N atom of the pyridine ring and the two O atoms of the carboxamide side arms of $\mathbf{L^9}$ is straightforward for heavy Ln^{III} ions, but induces some steric constraints for larger cations. Based on the significant tilts of the weakly bound pyridine rings in $[La(\mathbf{L^9})_3]^{3+}$, we conclude that the optimization of the six strong Ln–O bonds is associated with a weakening of the Ln–N bonds to accommodate the larger Ln^{III} ions. Such secondary weak, but significant effects are crucial for the thermodynamic recognition of Ln^{III} ions according to their size, if these interactions are maintained in solution.[14, 19, 49] For $[Ln(\mathbf{L^9})_3]^{3+}$, the detailed NMR investigation reported here confirms that related triple-helical structures are found in solution. For small cations (Ln = Er–Lu), the expected D_3-symmetrical structure is observed at room temperature, while a relaxed average D_{3h}-symmetrical structure is exhibited for the larger ones (Ln = La–Tb) as a result of fast $P \rightleftharpoons M$ helical interconversion on the NMR timescale. The analysis of variable-temperature NMR spectra suggest that the energy barriers of helical interconversion in $[Ln(\mathbf{L^9})_3]^{3+}$ are correlated with the magnitude of the interaction between Ln^{III} and the coordinated pyridine ring. The thermodynamic study in acetonitrile demonstrates that there is a monotonous increase in the stability of $[Ln(\mathbf{L^9})_3]^{3+}$ with decreasing Ln^{III} ionic radii, but the rather large uncertainties associated with the spectrophotometric determination of $\log(\beta_3)$ prevent smaller effects from being detected.

As far as luminescence is concerned, $[Ln(\mathbf{L^9})_3]^{3+}$ (Ln = Eu, Tb) building blocks are of only limited interest compared to $[Ln(\mathbf{L^{10}}-2H)_3]^{3-}$. Despite efficient $\mathbf{L^9} \rightarrow Ln^{III}$ energy transfers in the complexes, the coordinated ligand $\mathbf{L^9}$ displays only poor light-harvesting properties, which are not suitable for the development of efficient luminescent probes. We conclude that the "magic" luminescent enhancement associated with the introduction of carboxamide side arms in Tb-containing calixarenes[29] and in noncovalent lanthanide podates $[EuZn(\mathbf{L^7})_3]^{5+}$ is not a general process, but depends on subtle electronic and structural properties. In $[EuZn(\mathbf{L^7})_3]^{5+}$, the large luminescence increase probably results from the removal of low-energy excimer states associated with the wrapped bis(benzimidazolepyridine) strands in $[EuZn(\mathbf{L^6})_3]^{5+}$.[19, 49] The design of mononuclear lanthanide triple-helical building blocks derived from tridentate disubstituted 2,6-pyridine receptors possessing optimized thermodynamic, structural, and electronic properties will thus require the combination of carboxamide and extended aromatic side arms leading to unsymmetrical tridentate binding units. A close control of the expected *fac*↔*mer* isomerization in the final triple-helical complex must be addressed with the use of tripods to organize the strands for their coordination to Ln^{III} ions.

Experimental Section

Solvents and starting materials: These were purchased from Fluka AG (Buchs, Switzerland) and used without further purification unless otherwise stated. Acetonitrile was distilled twice from CaH_2 and thionyl chloride from elemental sulfur; *N*,*N*-dimethylformamide (DMF) and *N*,*N*-diethylamine were distilled from CaH_2. The perchlorate salts $Ln(ClO_4)_3\cdot nH_2O$ and trifluoromethanesulfonate salts $Ln(TfO)_3\cdot nH_2O$ (Ln = La to Lu) were prepared from the corresponding oxides (Glucydur, 99.99%) according to literature procedures.[60]

Preparation of *N*,*N*,*N*′,*N*′-tetraethylpyridine-2,6-dicarboxamide ($\mathbf{L^9}$): 2,6-Pyrididinedicarboxylic acid ($\mathbf{L^{10}}$, 10.0 g, 0.060 mol) was refluxed in freshly distilled thionyl chloride (100 mL, 1.37 mol) with dry DMF (1 mL) for 1 h. Excess thionyl chloride was evaporated, and the crude residue co-evaporated with dichloromethane (50 mL). The solid residue was dissolved in dichloromethane (250 mL) at 0 °C, and dry *N*,*N*-diethylamine (22.2 g, 0.60 mol) was added dropwise under an inert N_2 atmosphere. The resulting solution was refluxed for 1 h and evaporated. The yellow residue was partitioned between dichloromethane (200 mL) and half-saturated aqueous NH_4Cl solution (150 mL). The aqueous phase was extracted with dichloromethane (2 × 100 mL), the combined organic phase dried (Na_2SO_4) and evaporated, and the resulting solid filtered (Alox Activity III; CH_2Cl_2:MeOH = 98:2), then crystallized from hexane to give 15.3 g (0.055 mol, yield = 92%) of $\mathbf{L^9}$ as white crystals, mp = 74–76 °C (litt. 75 °C).[32] EI-MS: m/z = 277 [M^+].

Preparation of $[La(\mathbf{L^9})_3](ClO_4)_3$ (1): $La(ClO_4)_3\cdot 5.4H_2O$ (20 mg, 0.04 mmol) and $\mathbf{L^9}$ (41.6 mg, 0.15 mmol) were dissolved in propionitrile (5 mL). Diethyl ether was slowly diffused into the solution for 24 h to give 60 mg (0.039 mmol, yield = 98%) of $[La(\mathbf{L^9})_3](ClO_4)_3$ (**1**) as a white powder after isolation and drying.

Preparation of $[Ln(\mathbf{L^9})_3](TfO)_3\cdot H_2O$ (Ln = Y, 2; Sm, 4; Eu, 5; Gd, 6; Tb, 7; Lu, 3): $Ln(TfO)_3\cdot nH_2O$ (0.08 mmol; Ln = Sm, Eu, Gd, Tb, Lu, Y) and $\mathbf{L^9}$ (67.2 mg, 0.24 mmol) were dissolved in a minimum of hot THF (ca. 5–8 mL) and slowly cooled to room temperature. Crystallization took place at −20 °C over 8 h. After filtration and drying, complexes $[Ln(\mathbf{L^9})_3](TfO)_3\cdot H_2O$

(Ln = Y, **2**; Sm, **4**; Eu, **5**; Gd, **6**; Tb, **7**; Lu, **3**) were obtained as white microcrystalline powders in 80–92% yields.

X-ray quality crystals of $[La(L^9)_3](ClO_4)_3\cdot 2.5C_2H_5CN$ (8) and $[Eu(L^9)_3](TfO)_3\cdot 2THF$ (9) were obtained by the same procedures, but the prisms were not separated from the mother liquor. When separated, the prisms are readily transformed into a microcrystalline powder whose elemental analysis and IR spectrum are compatible with the formulation of **5** and **1**, respectively.

Preparation of $[Ln(L^9)(NO_3)_3]$ (Ln = Eu, 10; Tb, 11): $Ln(NO_3)_3\cdot nH_2O$ (0.225 mmol) and L^9 (62.5 mg, 0.225 mmol) were dissolved in acetonitrile (Ln = Tb, 2 mL) or propionitrile (Ln = Eu, 2 mL). Slow diffusion of diethyl ether into the solution gave white microcrystalline complexes $[Eu(L^9)(NO_3)_3](C_2H_5CN)_{0.5}(C_4H_{10}O)_{0.25}$ (**10**) and $[Tb(L^9)(NO_3)_3](CH_3CN)_{0.25}(C_4H_{10}O)_{0.5}$ (**11**) in 82% yield.

Complexes **1**–**7** and **10**–**11** were characterized by their IR spectra and gave satisfactory elemental analyses (Table S6 in the Supporting information). For the purpose of the photophysical study, Eu-doped La (**1a**), Gd (**6a**) and Lu (**3a**) complexes were prepared by replacing the pure lanthanide compound with an Eu(2%)–Ln(98%) mixture.

Preparation of $[Ln(L^9)_3](TfO)_3$ (Ln = Ce, Pr, Nd, Er, Tm, Yb): These complexes were prepared in situ for ^{1}H NMR studies. $Ln(TfO)_3\cdot nH_2O$ (0.036 mmol; Ln = Ce, Pr, Nd, Er, Tm, Yb; $n = 0.5$–2.2) and L^9 (30 mg, 0.108 mmol) were dissolved in degassed CD_3CN (0.7 mL) to give a 0.05 M solution of $[Ln(L^9)_3](TfO)_3$, the purity of which was checked by ^{1}H NMR spectroscopy.

Caution! Perchlorate salts with organic ligands are potentially explosive and should be handled with the necessary precautions.[61]

Crystal structure determination of $[La(L^9)_3](ClO_4)_3\cdot 2.5C_2H_5CN$ (8): A fragile crystal was mounted from the mother liquor on a quartz fiber with perfluoropolyether oil RS3000[®].

Crystal data: $LaC_{52.5}H_{81.5}N_{11.5}O_{18}Cl_3$, $M_r = 1407$, triclinic, $P\bar{1}$, $a = 12.930(1)$, $b = 13.531(1)$, $c = 18.877(3)$ Å, $\alpha = 90.209(5)$, $\beta = 90.459(6)$, $\gamma = 90.130(3)^\circ$, $U = 3302.5(6)$ Å^3 (by least-squares refinement of 22 reflections, $41 \le 2\theta \le 56^\circ$), $Z = 2$, $\rho_{calcd} = 1.42$ g cm^{-3}, $F(000) = 1458$. Colorless prisms. Crystal dimensions $0.06 \times 0.24 \times 0.25$ mm, $\mu(Cu_{K\alpha}) = 6.74$ mm^{-1}.

Data collection and processing: Nonius CAD4 diffractometer, $T = 170$ K, ω–2θ scan, scan width $= 1.5 + 0.14\tan\theta$, scan speed 0.092° s^{-1}, $Cu_{K\alpha}$ radiation ($\lambda = 1.5418$ Å); 7666 reflections measured ($4 \le 2\theta \le 106^\circ$, $-13 < h < 13$, $-14 < k < 14$, $0 < l < 19$), 6534 were observable ($|F_o| > 4\sigma(F_o)$). Two reference reflections were measured every 100 reflections and showed a total decrease in intensity of 5%. All intensities were corrected for this drift.

Structure analysis and refinement: Data were corrected for Lorentz, polarization and absorption effects[62] ($A^*_{min} = 1.494$, $A^*_{max} = 4.205$). The structure was solved by direct methods using multan 87;[63] all other calculations used XTAL[64] system and ORTEP II[36] programs. Full-matrix least-squares refinements (on F) using weights of $\omega = 1/\sigma^2(F_o)$ gave final values $R = 0.062$, $R_\omega = 0.048$, for 796 variables and 6524 contributing reflections. The ethyl residue C9c–C10c and perchlorate f are disordered and were refined with restraints on bond length and bond angles with various population parameters. Two solvent molecules were located in general positions and refined with no restraints while the third propionitrile is disordered and located about an inversion center (0, $^1/_2$, $^1/_2$). The disordered non-H atoms of solvent molecules and perchlorate anions were refined with isotropic displacement parameters, and all the other atoms (86) with anisotropic displacement parameters. H atoms were placed in calculated positions and contributed to F_c calculations. The final Fourier difference synthesis showed a maximum of $+0.98$ and a minimum of -1.49 e Å^{-3}.

Crystal structure determination of $[Eu(L^9)_3](TfO)_3\cdot 2THF$ (9): A fragile crystal was mounted from the mother liquor on a quartz fiber with perfluoropolyether oil RS3000[®].

Crystal data: $EuC_{56}H_{85}N_9O_{17}F_9S_3$, $M_r = 1575.5$, monoclinic, $C2/c$, $a = 13.5619(4)$, $b = 23.097(1)$, $c = 22.438(1)$ Å, $\beta = 91.323(2)^\circ$, $U = 7026.5(5)$ Å^3 (by least-squares refinement of 25 reflections, $46 \le 2\theta \le 58^\circ$), $Z = 4$, $\rho_{calcd} = 1.49$ g cm^{-3}, $F(000) = 3248$. Colorless prisms. Crystal dimensions $0.15 \times 0.20 \times 0.22$ mm, $\mu(Cu_{K\alpha}) = 7.75$ mm^{-1}.

Data collection and processing: Nonius CAD4 diffractometer, $T = 200$ K, ω–2θ scan, scan width $= 1.5 + 0.14\tan\theta$, scan speed 0.092° s^{-1}, $Cu_{K\alpha}$ radiation ($\lambda = 1.5418$ Å); 4531 reflections measured ($4 \le 2\theta \le 110^\circ$, $-14 < h < 14$, $0 < k < 24$, $0 < l < 23$), 4402 unique reflections (R_{int} for equivalent reflections = 0.039) of which 3898 were observable ($|F_o| > 4\sigma(F_o)$). Two reference reflections were measured every 100 reflections and showed a variation in intensity $< 2.9\sigma(I)$.

Structure analysis and refinement: Data were corrected for Lorentz, polarization and absorption effects for spherical crystals[62] ($A^*_{min} = 3.22$, $A^*_{max} = 3.93$). The structure was solved by direct methods as described for **8**. Full-matrix least-squares refinements (on F) using weights of $\omega = 1$ gave final values $R = R_\omega = 0.058$, for 472 variables and 3887 contributing reflections. The molecule is located about a twofold axis with Eu, N1b, and C3b in special position 4e. One triflate is in a general position and displays disordered fluorine atoms, and one lies about an inversion center (4a). The anions were refined with restraints on bond distances and angles. The two solvent molecules are located on twofold axis (4e). The non-H atoms were refined with anisotropic displacement parameters (55 atoms). H atoms were placed in calculated positions and contributed to F_c calculations. The final Fourier difference synthesis showed a maximum of $+1.17$ and a minimum of -1.08 e Å^{-3}.

Crystallographic data (excluding structure factors) for the structures reported in this paper have been deposited with the Cambridge Crystallographic Data Centre as supplementary publication no. CCDC-100252. Copies of the data can be obtained free of charge on application to The Director, CCDC, 12 Union Road, Cambridge CB21EZ, UK (Fax: Int. code +(1223)336-033; e-mail: deposit@chemcrys.cam.ac.uk).

Spectroscopic and analytical measurements: Electronic spectra were recorded at 20 °C from 10^{-3} mol dm^{-3} solutions in CH_3CN with Perkin-Elmer Lambda 2, 5, and 7 spectrometers using quartz cells of 0.1 and 1 cm path length. Spectrophotometric titrations were performed with a Perkin-Elmer Lambda 5 spectrophotometer connected to an external computer. In a typical experiment, 50 mL of ligand (L^9) in acetonitrile (10^{-4} M) were titrated at 20 °C with a solution of $Ln(TfO)_3\cdot nH_2O$ 10^{-3} M in CH_3CN. After each addition of 0.20 mL, the absorbances at 13 wavelengths (220–310 nm) were recorded using a 1.0 cm quartz cell and transferred to the computer. Factor analysis and stability constant determination were carried out as previously described.[25] IR spectra were obtained from KBr pellets with a Perkin Elmer 883 spectrometer. ^{1}H NMR spectra were recorded at 25 °C on a Broadband Varian Gemini 300 spectrometer. Chemical shifts are given in ppm with respect to TMS. EI-MS (70 eV) were recorded with VG-7000E and Finnigan-4000 instruments. Pneumatically-assisted electrospray (ES-MS) mass spectra were recorded from 10^{-4} M acetonitrile solutions on an API 300 tandem mass spectrometers (PE Sciex) by infusion at 4–10 μL min^{-1} as previously described.[25] The experimental procedures for high-resolution, laser-excited luminescence measurements have been published previously.[65] Emission spectra in solution were recorded on a Perkin-Elmer LS-50 spectrometer, and the relative quantum yields were calculated using the formula given in Equation (15),[18] where subscript r stands for the reference and x for the samples:

$$Q_x/Q_r = \langle A_r(\lambda_r)/A_x(\lambda_x)\rangle \langle I(\lambda_r)/I(\lambda_x)\rangle \langle n_x^2/n_r^2\rangle \langle D_x/D_r\rangle \qquad (15)$$

A is the absorbance at the excitation wavelength, I is the intensity of the excitation light at the same wavelength, n is the refractive index (1.341 for all solutions in acetonitrile), and D is the measured integrated luminescence intensity. Cyclic voltammograms were recorded using a BAS CV-50 W potentiostat connected to a personal computer. A three-electrode system consisting of a stationary Pt disk working electrode, a Pt counter electrode, and a nonaqueous Ag/AgCl reference electrode was used. NBu_4PF_6 (0.1 M in CH_3CN) served as an inert electrolyte. The reference potential ($E^0 = -0.12$ V vs. SCE) was standardized against $[Ru(bipy)_3](ClO_4)_2$ (bipy = 2,2′-bipyridyl).[66] The scan speed was 100 mV s^{-1} and voltammograms were analyzed according to established procedures.[66] Elemental analyses were performed by Dr. H. Eder from the Microchemical Laboratory of the University of Geneva. Metal contents were determined by ICP (Perkin Elmer Plasma 1000) using internal standard techniques after mineralization of the complexes.

Acknowledgments: We gratefully acknowledge V. Foiret and S. Petoud for their assistance in recording the luminescence data. C. P. thanks the Werner Foundation for a fellowship and J.-C. B. thanks the Fondation Herbette

  0947-6539/97/0310-1658 $ 17.50+.50/0

(Lausanne) for the gift of spectroscopic equipment. This work is supported through grants from the Swiss National Science Foundation.

Supporting information is available from the correspondence author. Tables S1–6 list the ES-MS peaks observed during titration (S1), complete contact and pseudo-contact contributions to the NMR paramagnetic shifts of $[Ln(L^9)_3]^{3+}$ obtained from Equation (7) (S2) and Equation (12) (S3–S4), integrated luminescence intensities of complex **5** under various experimental conditions (S5), and elemental analyses of complexes **1**–**11** (S6). Figure F1 shows emission spectra of complexes **5**, **9**, and doped Eu(2%)-La and Eu(2%)-Gd compounds.

Received: March 14, 1997 [F640]

[1] J.-C. G. Bünzli in *Lanthanide Probes in Life, Chemical and Earth Sciences* (Eds.: J.-C. G. Bünzli, G. R. Choppin), Elsevier, Amsterdam, **1989**, Chapt. 7. J.-C. G. Bünzli, P. Froidevaux, C. Piguet, *New J. Chem.* **1995**, *19*, 661–668 and references therein.

[2] D. Parker, J. A. Gareth Williams, *J. Chem. Soc. Dalton Trans.* **1996**, 3613–3628.

[3] G. Mathis, *Clin. Chem.* **1993**, *39*, 1953–1959. G. Mathis, *Clin. Chem.* **1995**, *41*, 1391–1397.

[4] J. Coates, P. G. Sammes, R. M. West, *J. Chem. Soc. Chem. Commun.* **1995**, 1107–1108. P. R. Selvin, T. M. Rana, J. E. Hearst, *J. Am. Chem. Soc.* **1994**, *116*, 6029–6030.

[5] S. Aime, M. Botta, D. Parker, J. A. Gareth Williams, *J. Chem. Soc. Dalton Trans.* **1996**, 17–23; *ibid.* **1995**, 2259–2266; D. H. Powell, M. Favre, N. Graeppi, O. M. Ni Dhubhghaill, D. Pubanz, A. E. Merbach, *J. Alloys Compds*, **1995**, *225*, 246–252; K. Kumar, M. F. Tweedle, *Pure Appl. Chem.* **1993**, *65*, 515–520; R. B. Lauffer, *Chem. Rev.* **1987**, *87*, 901–927.

[6] R. Hazama, K. Umakoshi, C. Kabuto, K. Kabuto, Y. Sasaki, *Chem. Commun.* **1996**, 15–16.

[7] J. Hall, D. Hüsken, U. Pieler, H. E. Moser, R. Häner, *Chem. Biol.* **1994**, *1*, 185–190. T. C. Bruice, A. Tsubouchi, R. O. Dempcy, L. P. Olson, *J. Am. Chem. Soc.* **1996**, *118*, 9867–9875. P. Hurst, B. T. Takasaki, J. Chin, *J. Am. Chem. Soc.* **1996**, *118*, 9982–9983.

[8] G. R. Choppin in *Lanthanide Probes in Life, Chemical and Earth Sciences* (Eds.: J.-C. G. Bünzli, G. R. Choppin), Elsevier, Amsterdam, **1989**, Chapt. 1.

[9] F. W. Lichtenthaler, *Angew. Chem. Int. Ed. Engl.* **1994**, *33*, 2364–2374.

[10] N. Sabbatini, M. Guardigli, J.-M. Lehn, *Coord. Chem. Rev.* **1993**, *123*, 201–228 and references therein.

[11] C. O. Paul-Roth, J.-M. Lehn, J. Guilhem, C. Pascard, *Helv. Chim. Acta* **1995**, *78*, 1895–1903. F. Bodar-Houillon, A. Marsura, *New J. Chem.* **1996**, *20*, 1041–1045.

[12] C. Galaup, C. Picard, L. Cazaux, L. P. Tisnès, D. Aspe, H. Autiero, *New J. Chem.* **1996**, *20*, 997–999.

[13] V. Balzani, E. Berghmans, J.-M. Lehn, N. Sabbatini, R. Terörde, R. Ziessel, *Helv. Chim. Acta* **1990**, *73*, 2083–2089.

[14] P. Caravan, T. Hedlund, S. Liu, S. Sjöberg, C. Orvig, *J. Am. Chem. Soc.* **1995**, *117*, 11230–11238.

[15] U. Casellato, S. Tamburini, P. Tomasin, P. A. Vigato, M. Botta, *Inorg. Chim. Acta* **1996**, *247*, 143–145.

[16] D. A. Koshland, *Angew. Chem. Int. Ed. Engl.* **1994**, *33*, 2375–2378.

[17] C. Piguet, A. F. Williams, G. Bernardinelli, J.-C. G. Bünzli, *Inorg. Chem.* **1993**, *32*, 4139–4149.

[18] C. Piguet, J.-C. G. Bünzli, G. Bernardinelli, C. G. Bochet, P. Froidevaux, *J. Chem. Soc. Dalton Trans.* **1995**, 83–97.

[19] S. Petoud, J.-C. G. Bünzli, F. Renaud, C. Piguet, *J. Alloys and Compounds* **1997**, *249*, 14–24.

[20] C. Piguet, B. Bocquet, G. Hopfgartner, *Helv. Chim. Acta* **1994**, *77*, 931–942.

[21] C. Piguet, J.-C. G. Bünzli, G. Bernardinelli, G. Hopfgartner, A. F. Williams, *J. Am. Chem. Soc.* **1993**, *115*, 8197–8206.

[22] C. Piguet, G. Hopfgartner, A. F. Williams, J.-C. G. Bünzli, *J. Chem. Soc. Chem. Commun.* **1995**, 491–493; C. Piguet, E. Rivara-Minten, G. Hopfgartner, J.-C. G. Bünzli, *Helv. Chim. Acta* **1995**, *78*, 1541–1566.

[23] C. Piguet, E. Rivara-Minten, G. Hopfgartner, J.-C. G. Bünzli, *Helv. Chim. Acta* **1995**, *78*, 1651–1672.

[24] C. Piguet, G. Bernardinelli, J.-C. G. Bünzli, S. Petoud, G. Hopfgartner, *J. Chem. Soc. Chem. Commun.* **1995**, 2575–2577.

[25] C. Piguet, J.-C. G. Bünzli, G. Bernardinelli, G. Hopfgartner, S. Petoud, O. Schaad, *J. Am. Chem. Soc.* **1996**, *118*, 6681–6697.

[26] I. Grenthe, *J. Am. Chem. Soc.* **1961**, *83*, 360–364. P. A. Brayshaw, J.-C. G. Bünzli, P. Froidevaux, J. M. Harrowfield, Y. Kim, A. N. Sobolev, *Inorg. Chem.* **1995**, *34*, 2068–2076. J. M. Harrowfield, Y. Kim, B. W. Skelton, A. H. White, *Aust. J. Chem.* **1995**, *48*, 807–823 and references therein. J. B. Lamture, Z. Zhou, S. Kumar, T. G. Wenzel, *Inorg. Chem.* **1995**, *34*, 864–869.

[27] C. N. Reilley, B. W. Good, J. F. Desreux, J. F. *Anal Chem.* **1975**, *47*, 2110–2116.

[28] E. Huskowska, J.-P. Riehl, *Inorg. Chem.* **1995**, *34*, 5615–5621 and references therein.

[29] N. Sabbatini, M. Guardigli, A. Mecati, V. Balzani, R. Ungaro, E. Ghidini, A. Casnati, A. Pochini, *J. Chem. Soc. Chem. Commun.* **1990**, 878–879. D. M. Rudkevich, W. Verboom, E. van der Tal, C. J. van Staveren, F. M. Kasparen, J. W. Verhoeven, D. N. Rheinhoudt, *J. Chem. Soc. Perkin Trans. 2* **1995**, 131–134. J. H. Forsberg, R. M. Delanoy, Q. Zhao, G. Harakas, R. Chandron, *Inorg. Chem.* **1995**, *34*, 3705–3715.

[30] M. Li, P. R. Selvin, *J. Am. Chem. Soc.* **1995**, *117*, 8132–8138.

[31] J. Garcia-Lozano, L. Soto, J.-V. Folgado, E. Escriva, *Polyhedron* **1996**, *15*, 4003–4009. J. Garcia-Lozano, M. A. Martinez-Lorente, E. Escriva, R. Ballesteros, *Synth. React. Inorg. Met.-Org. Chem.* **1994**, *24*, 365–376. J. G. H. DuPreez, B. J. A. M. van Brecht, *Inorg. Chim. Acta* **1989**, *162*, 49–56.

[32] R. Jagannathan, S. Soundararajan, *Indian J. Chem. Sect. A* **1979**, *18A*, 319–321. R. Jagannathan, S. Soundararajan, *J. Coord. Chem.* **1979**, *9*, 31–35.

[33] S. Rüttimann, C. Piguet, G. Bernardinelli, B. Bocquet, A. F. Williams, *J. Am. Chem. Soc.* **1992**, *114*, 4230–4237.

[34] J.-L. Pascal, M. E. M. Hamidi, *Polyhedron*, **1994**, *13*, 1787–1792.

[35] K. Nakamoto, *Infrared and Raman Spectra of Inorganic and Coordination Compounds*, 3rd ed.; Wiley, New York, **1972**, p. 142.

[36] C. K. Johnson, *ORTEP II; Report ORNL-5138*; Oak Ridge National Laboratory, Oak Ridge, Tennessee, **1976**.

[37] C. Paul-Roth, K. N. Raymond, *Inorg. Chem.* **1995**, *34*, 1408–1412. S. Amin, D. A. Voss, W. de W. Horrocks, C. H. Lake, M. R. Churchill, J. R. Morrow, *Inorg. Chem.* **1995**, *34*, 3294–3300. S. J. Franklin, K. N. Raymond, *Inorg. Chem.* **1994**, *33*, 5794–5804.

[38] R. D. Shannon, *Acta Cryst.* **1976**, *A32*, 751–767.

[39] C. Piguet, G. Bernardinelli, G. Hopfgartner, *Chem. Rev.* **1997**, submitted.

[40] S. T. Frey, W. de W. Horrocks, *Inorg. Chim. Acta* **1995**, *229*, 383–390.

[41] W. de W. Horrocks, D. R. Sudnick, *J. Am. Chem. Soc.* **1979**, *101*, 334–340. W. de W. Horrocks, D. R. Sudnick, *Science* **1979**, *206*, 1194–1196. W. de W. Horrocks, D. R. Sudnick, *Acc. Chem. Res.* **1981**, *14*, 384–392.

[42] G. Hopfgartner, C. Piguet, J. D. Henion and A. F. Williams, *Helv. Chim. Acta*, 1993, **76**, 1759–1766; G. Hopfgartner, C. Piguet, J. D. Henion, *J. Am. Soc. Mass Spectrom.* 1994, **5**, 748–756.

[43] N. N. Greenwood, A. Earnshaw, *Chemistry of the Elements*, Pergamon Press, Oxford, **1986**, p. 1431.

[44] E. Leize, A. Jaffrezic, A. Van Dorsselaer, *J. Mass Spectrom.* **1996**, *31*, 537–544.

[45] E. R. Malinowski, D. G. Howery, *Factor Analysis in Chemistry*, Wiley, New York, **1980**.

[46] P. H. Smith, Z. E. Reyes, C. W. Lee, K. N. Raymond, *Inorg. Chem.* **1988**, *27*, 4154–4165.

[47] J. Massaux, G. Duyckaerts, *Anal. Chim. Acta* **1974**, **73**, 416–419.

[48] C. Piguet, E. Rivara-Minten, G. Bernardinelli, J.-C. G. Bünzli, G. Hopfgartner, *J. Chem. Soc. Dalton Trans.* **1997** 421–433.

[49] S. Petoud, J.-C. G. Bünzli, K. Schenk, C. Piguet, F. Renaud, unpublished results.

[50] C. Piguet, G. Hopfgartner, B. Bocquet, O. Schaad, A. F. Williams, *J. Am. Chem. Soc.* **1994**, *116*, 9092–9102. D. K. Lavallee, M. D. Baughan, M. P. Phillips, *ibid.* **1977**, *99*, 718–724.

[51] H. Günther, *NMR Spectroscopy*, Wiley, Chichester, **1980**, p. 243.

[52] I. Bertini, C. Luchinat, *NMR of Paramagnetic Molecules in Biological Systems*, Benjamin/Cummings, Menlo Park, CA., **1986**, Chapt. 10. I. Bertini, P. Turano, A. J. Vila, *Chem. Rev.* **1993**, *93*, 2833–2932.

[53] R. M. Golding, M. P. Halton, *Aust. J. Chem.* **1972**, *25*, 2577–2581.

[54] B. J. Bleaney, *J. Magn. Reson.* **1972**, *8*, 91–100. J. Reuben, G. A. Rigavish, *ibid.* **1980**, *39*, 421–430.

[55] M. D. Kemple, B. D. Ray, K. B. Lipkowitz, F. G. Prendergast, B. D. N. Rao, *J. Am. Chem. Soc.* **1988**, *110*, 8275–8287.

[56] A. D. Sherry, C. F. G. C. Geraldes in *Lanthanide Probes in Life, Chemical and Earth Sciences* (Eds.: J.-C. G.Bünzli, G. R. Choppin), Elsevier, Amsterdam, **1989**, Chapt. 4. T. Nakamura, C. Miyake, *J. Alloys and Compds* **1995**, *225*, 334–337.

[57] J. M. Brink, R. A. Rose, R. C. Holz, *Inorg. Chem.* **1996**, *35*, 2878–2885.

[58] S. Petoud, J.-C. G. Bünzli, K. J. Schenk, C. Piguet, *Inorg. Chem.* **1997**, *36*, 1345–1353.

[59] K. Nakamura, *Bull. Chem. Soc.* Jpn **1982**, *55*, 2697–2705.

[60] J. F. Desreux in *Lanthanide Probes in Life, Chemical and Earth Sciences* (Eds.: J.-C. G. Bünzli and G. R. Choppin), Elsevier, Amsterdam, **1989**, Chapt. 2, p. 43.

[61] W. C. Wolsey, *J. Chem. Educ.* **1978**, *55*, A355.

[62] E. Blanc, D. Schwarzenbach, H. D. Flack, *J. Applied Crystallogr.* **1991**, *24*, 1035–1041.

[63] P. Main, S. J.Fiske, S. E. Hull, L. Lessinger, D. Germain, J. P. Declercq, M. M. Woolfson, *MULTAN 87*; Universities of York (UK) and Louvain-La-Neuve (Belgium), **1987**.

[64] S. R. Hall, J. M. Stewart, Eds. *XTAL 3.2 User's Manual*; Universities of Western Australia and Maryland, **1992**.

[65] C. Piguet, A. F. Williams, G. Bernardinelli, E. Moret, J.-C. G. Bünzli, *Helv. Chim. Acta* 1992, **75**, 1697–1717.

[66] A. J. Bard, L. R. Faulkner, *Electrochemical Methods, Fundamentals and Application*, Wiley, New York, **1980**.